Quantifying nutrient colimitation of microbial growth

Noelle A. Held*
Institute of Biogeochemistry and Pollutant Dynamics, Department of Environmental Systems Science, ETH Zurich, Zurich, Switzerland and Department of Environmental Microbiology, Swiss Federal Institute of Aquatic Science and Technology (Eawag), Dübendorf, Switzerland

Aswin Krishna
Department of Biology, ETH Zurich, Zurich Switzerland

Donat Crippa
Department of Environmental Systems Science, ETH Zurich, Zurich, Switzerland

Anastasia Dragan
Institute of Integrative Biology, Department of Environmental Systems Science, ETH Zurich, Zurich, Switzerland

Michael Manhart†
Institute of Integrative Biology, Department of Environmental Systems Science, ETH Zurich, Zurich, Switzerland Department of Environmental Microbiology, Swiss Federal Institute of Aquatic Science and Technology (Eawag), Dübendorf, Switzerland and Center for Advanced Biotechnology and Medicine and Department of Biochemistry and Molecular Biology, Robert Wood Johnson Medical School, Rutgers University, Piscataway, NJ, USA

(Dated: September 27, 2023)

Nutrient availability dictates how fast and how much microbial populations grow. Quantifying the relationship between microbial growth and nutrient concentrations makes it possible to promote, inhibit, and predict microbial activity. Microbes require many different resources, including elemental nutrients such as carbon, nitrogen, and the trace metals, as well as complex nutrients like vitamins and amino acids. In nature, many of these nutrients are scarce and their abundances co-vary. This presents the possibility of nutrient colimitation, when more than one resource limits growth simultaneously. Despite growing evidence of possible colimitation in nature, the data is often difficult to interpret and compare due to lack of quantitative definitions for limitation and colimitation. Here we introduce a set of metrics that quantify multiple nutrient limitation in microbial growth. We introduce the limitation coefficient to quantify limitation by individual resources and a colimitation index for measuring the effective number of limiting resources. These quantities demonstrate that limitation conditions are not binary or static, but rather exist on a continuum and can change over time as resource conditions change. These definitions facilitate quantitative comparisons between laboratory experiments and nutrient conditions in nature. Furthermore, they allow us to illustrate how limitation of microbial growth rate and biomass yield are related but distinct notions. To demonstrate these concepts, we measure growth of *Escherichia coli* under laboratory conditions and demonstrate that colimitation occurs in clonal populations and is readily accessible in laboratory conditions. Finally, we apply our framework to environmental data to provide intuition for what limitation conditions might exist in nature.

Keywords: microbial growth, resource limitation, colimitation, growth rate, marine microbes, biogeochemistry, biotechnology, *Escherichia coli*

INTRODUCTION

Nutrient availability controls the growth, physiology, and activity of microbes. Microbes need many nutrients to grow, and in nature many of these nutrients are simultaneously rare. A basic concept for modeling microbial growth in the context of multiple nutrients is Liebig's Law of the Minimum, which states that growth is determined by availability of the scarcest nutrient relative to biological demand. While Liebig's law was originally defined for agricultural plant yields, the idea has since been applied to other systems such as the growth of animals [1, 2], human populations [3], and microbes [4], the latter being the focus of this study.

Liebig's law of the minimum has largely defined experimentation and modeling of microbial growth in nutrient limitation. Ecosystem and biogeochemical models that incorporate nutrient limitation of microbial growth rates and biomass production often employ a minimizing func-

* To whom correspondence should be addressed. Email: nheld@usc.edu; Current address: Department of Biological Sciences, Marine & Environmental Biology Division, University of Southern California, Los Angeles, CA, USA

† To whom correspondence should be addressed. Email: mmanhart@rutgers.edu

tion [5–8]. In laboratory experiments, it is customary to designate a specific limiting nutrient, while keeping other nutrients in excess. This approach has demonstrated that the growth, physiology, and molecular biology of microorganisms are influenced by the identity of the limiting nutrient [9–13]. However, focusing on single, on/off nutrient limitations restricts our understanding and predictions of microbial growth in nature, where microbes experience a continuous range of nutrient concentrations and where many nutrients are simultaneously scarce [14–19].

There are hints that microbial growth could be, and in nature often is, simultaneously limited by multiple nutrients (nutrient colimitation). One line of evidence comes from biogeochemistry. In systems such as the open ocean, the elemental composition of the environment reflects that of abundant microbes suggesting a balance between supply and biological demand [19–21]. Accordingly, in situ factorial experiments in which nutrients are supplemented individually and in combinations sometimes find super-additive effects of adding multiple resources [16, 18, 22–26]. Nutrient colimitation has also been explored in laboratory experiments in which microbial populations drew down multiple resources simultaneously [27, 28]. Finally, in microbial communities, ecological theory predicts the coexistence of multiple species within a resource supply range, with each species depleting a specific resource, leading to colimitation of the community as a whole [29–32].

Though nutrient colimitation has been acknowledged since the earliest literature [33], a central question remains: Is nutrient colimitation an exception, or a rule? So far, interpretations have been limited by lack of a common quantitative framework. A range of models have been proposed, including the commonly used multiplicative model (a product of Monod functions) [15], Poisson arrival time (PAT) model [34], additive or Bloomfield model [34, 35], and others. Generally, these models are phenomenological in nature and not necessarily motivated from biological mechanisms. The variety of discrete models used in different studies means that the current literature lacks the ability to quantitatively assess the extent of nutrient colimitation as opposed to single nutrient, Liebig-type limitation [15, 17, 36].

In this study, we propose quantitative metrics that describe the phenomenon of nutrient-limited microbial growth including when growth depends on multiple nutrients simultaneously (colimitation). For illustration, we focus on the basic case of colimitation by biologically necessary, non-substitutable, independent nutrients such as carbon (C) and nitrogen (N), as opposed to when nutrients are substitutable or when there is a direct biochemical dependence (i.e., uptake of one nutrient is dependent on the other). To build a fundamental understanding of the phenomenon of nutrient colimitation, we concentrate on clonal populations rather than microbial communities.

The framework allows us to assess the extent of limitation and degree of nutrient colimitation, allowing a quantitative treatment of a problem that is usually restricted to qualitative interpretation. We demonstrate that colimitation of microbial growth rates and biomass production is accessible in laboratory conditions and relevant in nature. This allows us to conclude that the spectrum of microbial growth is best understood in the context of multiple nutrients.

RESULTS

Growth rate limitation is a quantitative, dynamic property of a microbial population. Let the growth rate of a microbial population be $g(R)$, depending on the concentration R of a resource in the environment. A classic example of this dependence is given by the Monod model [37, 38](Fig. 1A):

$$g(R) = g_{\max}\frac{R}{R+K}, \tag{1}$$

where $g_{\max}$ is the maximum growth rate when the resource concentration is infinite, and K is the half-saturation resource concentration where growth rate is half $g_{\max}$. Decreasing the half-saturation concentration K therefore allows the population to grow faster at lower resource concentrations. The Monod formula is the most commonly invoked model of microbial growth in nutrient limitation, and we focus on it here but note that our framework can be applied to any saturating model of growth rate.

We define the growth rate limitation coefficient for this resource as the relative change in growth rate for a small relative change in resource concentration (Fig. 1A):

$$L^{\text{rate}} = \frac{R}{g}\frac{\partial g}{\partial R}. \tag{2}$$

This quantity is defined in analogy with control coefficients in metabolic control analysis [39]. It can be applied to any model of microbial growth rates, and for most models including the Monod model, the limitation coefficient ranges from $L^{\text{rate}} = 0$ at infinite resource concentrations to $L^{\text{rate}} = 1$ at zero concentrations (Supplementary Information Sec. S1). For the Monod model with a single resource (Eq. 1), $L^{\text{rate}} = K/(R+K)$ (Fig. 1A). This limitation coefficient gives us a measure of limitation that is quantitative, rather than a binary state of the population as is often discussed (limiting or non-limiting). It is also dynamic: since it depends on the resource concentration (Fig. 1A), it changes over time as the resource increases or decreases, such as over the course of a batch culture.

Multiple resources can be absolutely or relatively colimiting. For growth rate that depends on M resources $g(R_1, R_2, \ldots, R_M)$, we can define limitation coefficients L_i^{rate} for each resource i using Eq. 2. We define *absolute colimitation* as when limitation coefficients L_i^{rate} and L_j^{rate} for two resources i and j are both large; Fig. 1B shows a schematic of these regimes over concentration

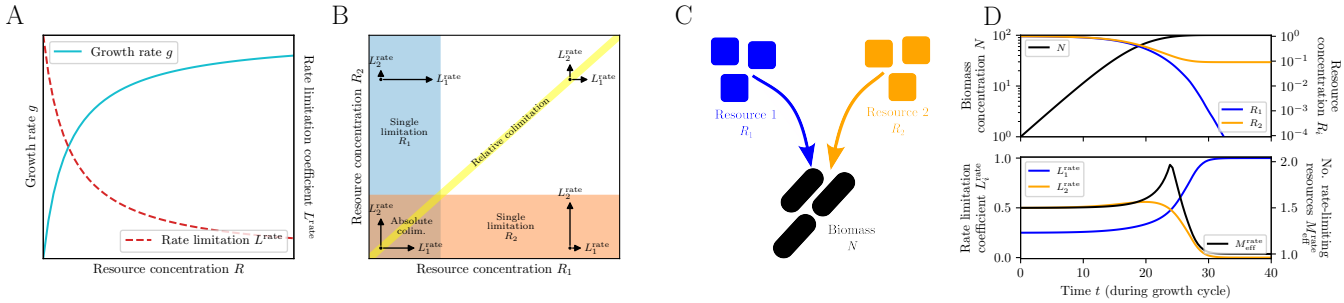

FIG. 1. **Resource limitation and colimitation of population growth rate.** (A) Schematic of growth rate $g(R)$ (solid cyan line) as a function of environmental resource concentration R. This is representative of the typical Monod-like dependence (Eq. 1) we assume in this article, as has been empirically measured [37, 38]. We also show the growth rate limitation coefficient $L^{\rm rate}(R)$ (dashed red line; Eq. 2) across the same resource concentrations. (B) Schematic of concentration space for two resources, showing different limitation conditions. The black arrows show limitation coefficients $L_i^{\rm rate}$ for each resource at different combinations of concentrations, and the shaded regions mark regions of high limitation for resource 1 (blue) and resource 2 (orange). The yellow diagonal band marks the approximate region of relative colimitation, where the number of limiting nutrients $M_{\rm eff}^{\rm rate}$ is close to 2. (C) Diagram for a model of biomass with concentration N consuming two resources with concentrations R_1 (blue) and R_2 (orange). (D) Simulation of batch culture dynamics for the model in (C). The top panel shows the growth of biomass (black line) as the two resources (blue and orange) are depleted over time. The bottom panel shows the limitation coefficients $L_i^{\rm rate}$ and the number of limiting resources $M_{\rm eff}^{\rm rate}$ over the same time range.

ranges for two resources. Here the blue region represents limitation for resource 1 (large $L_1^{\rm rate}$), while the orange region represents single limitation for resource 2 (large $L_2^{\rm rate}$). The overlap represents absolute colimitation for both resources.

Another property is *relative colimitation*, when limitation coefficients between multiple resources are of similar magnitude. This indicates which and how many nutrients should be considered in a microbial growth model. The distinction is important because the growth, physiology, and molecular properties of cells are dependent on the identity of the limiting nutrient(s), not just the degree of limitation [9]. Additionally, the growth response to a pulse or fluctuation in nutrients will depend both on the nature of the limitation and degree of limitation [40]. We quantify relative colimitation as the sum of limitation coefficients for all resources, normalized by the largest limitation coefficient:

$$M_{\rm eff}^{\rm rate} = \frac{\sum_{\text{resource } i} L_i^{\rm rate}}{\max_{\text{resource } i} L_i^{\rm rate}}. \tag{3}$$

It has a minimum value of $M_{\rm eff}^{\rm rate} = 1$ if only one resource has nonzero limitation coefficient, and a maximum value of $M_{\rm eff}^{\rm rate} = M$ (the total number of resources) if all resources have equal limitation. Therefore we can interpret $M_{\rm eff}^{\rm rate}$ as the effective number of relatively colimiting resources. This quantity is maximized along a diagonal region (yellow area in Fig. 1B) in the space of resource concentrations, where both resources are equally limiting. Note that this overlaps the region of absolute colimitation, but also extends to conditions where both resources are not limiting in absolute terms but still have similar relative limitation.

For example, consider a population consuming two essential resources, shown schematically in Fig. 1C. Figure 1D (top panel) shows the dynamics of the biomass and resource concentrations in a batch culture (Methods). The biomass concentration increases exponentially while the two resources are depleted. While the orange nutrient is at first more limiting, it is the blue resource that runs out first (bottom panel of Fig. 1D). At the point where the limitation coefficients cross over each other, the effective number of limiting resources $M_{\rm eff}^{\rm rate}$ equals exactly 2, since both resource are equally limiting. In Fig. S1 we show analogous scenarios for continuous cultures (chemostat), where resources are supplied to the population at constant rate (Supplementary Secs. S2 and S3).

Growth rate colimitation is readily accessible under laboratory conditions. To investigate these concepts quantitatively, we need to consider specific models of how growth rate depends on multiple resources, $g(R_1, R_2, \ldots, R_M)$. To start, we focus on the example of essential, non-substitutable resources like carbon and nitrogen sources. For these cases, researchers have used many models in the past, without consensus on which one is most accurate or whether they describe biologically different scenarios [2, 15, 28, 34–36]. We focus on four commonly-used models of growth rate (Fig. S2, first row; Methods and Supplementary Information Sec. S4): the Liebig model (also known as the "law of the minimum") [15, 28, 34], the Poisson arrival time (PAT) model [2, 34], the additive model (also known as the Bloomfield model) [2, 34], and the multiplicative model [2, 28, 36]. All four models share the same key properties: growth rate is zero if any resource is zero (all resources are essential); they reduce to the Monod model for a single resource (Eq. 1) if all other resources are un-

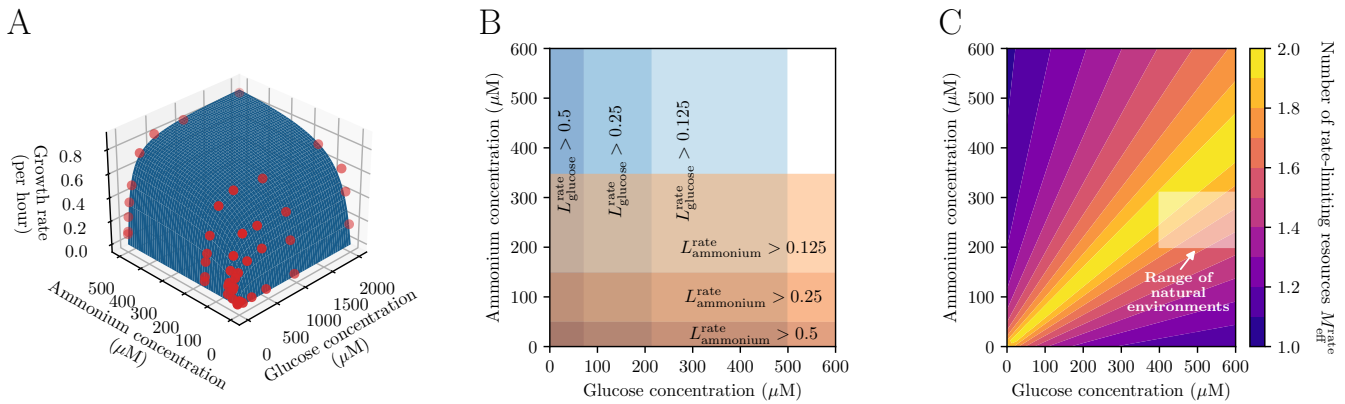

FIG. 2. **Experimental measurement of growth rate limitation and colimitation.** (A) Growth rate measurements (red points) over glucose and ammonium concentrations for *E. coli* in minimal medium (Methods, Dataset S1; see Figs. S5 and S6 for growth curves). The blue surface is the best-fit model (multiplicative model; Methods and Fig. S7; $g_{\max} \approx 1.0$ hour^{-1}, $K_{\text{glucose}} \approx 71$ μM, $K_{\text{ammonium}} \approx 50$ μM). (B) Using the model fitted in (A), we calculate regions of growth rate limitation coefficients L^{rate} (Eq. 2) for glucose (blue) and ammonium (orange) across concentrations. The overlap between these regions indicates conditions where both resources are absolutely colimiting (compare to Fig. 1B). (C) Using the model fitted in (A), we calculate growth rate colimitation of glucose and ammonium (number of limiting resources $M^{\text{rate}}_{\text{eff}}$, Eq. 3) across concentrations of both resources. The white box indicates the approximate range of glucose and ammonium concentrations found in natural environments for *E. coli* (Methods, Dataset S2).

limited; and they saturate at a finite maximum growth rate $g_{\max}$ is all resources are unlimited (Supplementary Sec. S4).

While the dependence of growth rate on resource concentration appears similar across these models (Fig. S2, first row), the models differ when we consider their limitation properties (Fig. S2, second and third rows). In particular, the models show a gradient of colimitation: the Liebig model has no colimitation by construction, whereas the multiplicative model has colimitation over the widest range of resource concentrations, with the PAT and additive models in between (Fig. S2 and Fig. S3). While here we focus on essential, non-substitutable resources like carbon and nitrogen sources, we can also extend this analysis to pairs of resources that are substitutable (e.g., different carbon sources or Type II colimitation [15]; Supplementary Information Sec. S5 and Fig. S4) or chemically-dependent (or Type III colimitation [15]; Supplementary Information Sec. S6 and Fig. S4).

To realize these colimitation conditions in the laboratory, we varied glucose and ammonium over ranges of concentrations and measured the growth rates of a clonal population of *Escherichia coli* under these conditions (Figs. 2, S5, and Fig. S6; Methods; Dataset S1). We fit each of the four growth rate models to this data (Fig. S7). The Liebig minimizing model performed worst in describing the data, and while all three non-Liebig models performed better and similarly, we found a slight preference for the multiplicative model. We used this best-fit model to calculate the limitation and colimitation regimes in Fig. 2B,C. This shows significant colimitation by glucose and ammonium ($M^{\text{rate}}_{\text{eff}} > 1$). The region of high colimitation overlaps with the estimated range of nutrient concentrations experienced by *E. coli* in nature (Fig. 2C; Methods; Dataset S2).

Quantifying growth rate colimitation across species and resources in natural environments. We have shown that colimitation can occur in the laboratory, but is it also realized in nature? To demonstrate this, we collected measurements of half-saturation resource concentrations K_i (measured from the dependence of growth rate on that resource concentration according to the Monod model [37]) and environmental concentrations R_i for those same resources across many organisms (Fig. 3A, Methods, Dataset S2).

We use this data to estimate limitation for each resource, assuming all other resources for these organisms are present at very high concentrations. Since the true dependence of growth rate on multiple resources is unknown for these organisms and resources, we test all four growth rate models from Fig. S2 to calculate limitation coefficients in Fig. 3B. We find significant limitation coefficients for many of the marine species, but low limitation for the freshwater and enteric species. This is evident from the R and K data itself; most half-saturation concentrations K are less than their corresponding environmental concentrations R, which means low limitation, with the exceptions being several marine strains on phosphate and nitrate (Fig. 3A).

Next we quantify relative colimitation between these resources using the number of limiting resources $M^{\text{rate}}_{\text{eff}}$ (Fig. 3C). While several of the marine species show high colimitation, we also see intermediate levels of colimitation for some enteric species, even though their absolute levels of limitation are low (Fig. 3B). While these esti-

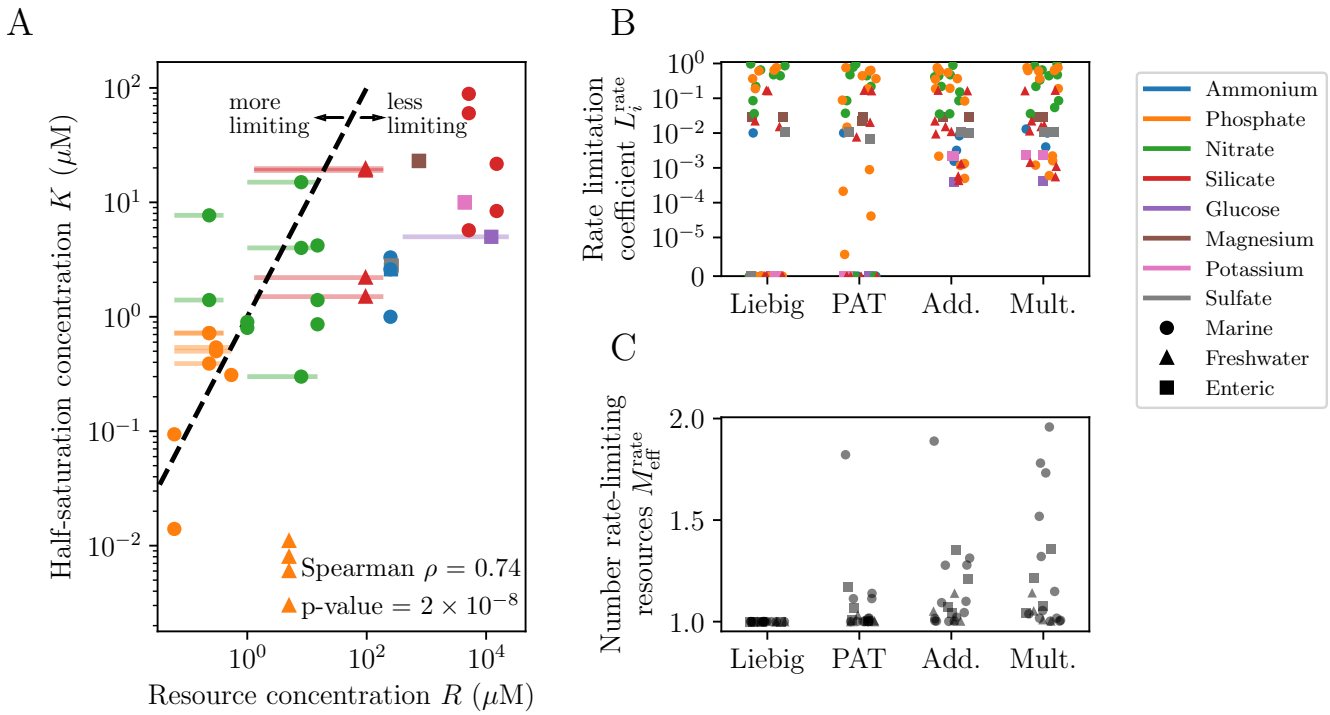

FIG. 3. **Applying growth rate limitation concepts to empirical data across species and resources.** (A) Representative half-saturation concentrations K (μM) versus environmental concentrations R (μM) for data from various organisms, resources, and environments collected from the literature (Dataset S2). When we found environmental concentrations R as ranges, we indicate this by horizontal bars in the plot. Scatter points are colored based on the resource being considered; marker shape indicates the habitat. The Spearman correlation coefficient between R and K is $\rho \approx 0.74$ with a p-value $\approx 2 \times 10^{-8}$. (B) Rate limitation coefficients (L_i^{rate}) calculated from the data shown in (A); we calculated limitation coefficients for individual resources in all organism/resource combinations, considering different growth rate models (horizontal axis: Liebig = Liebig model, PAT = Poisson arrival time model, Add. = additive model, Mult. = multiplicative Monod model; Methods, Supplementary Information Sec. S4). (C) Number of rate-limiting resources $M_{\text{eff}}^{\text{rate}}$ calculated from the data shown in (A), also considering the same growth rate models as in (B).

mates are limited by uncertainties in the parameters as well as exclusion of other resources for which we do not have data, we can show that the limitation coefficients are upper bounds on the extent of limitation and therefore that $M_{\text{eff}}^{\text{rate}}$ is not very sensitive to the inclusion of additional nutrients (Supplementary Information Sec. S7).

Dynamics of resource depletion. Besides affecting *how fast* a population grows (growth rate), resource concentrations also determine *how much* new biomass grows over a period of time (biomass yield). In Fig. 4A, consider a batch culture where resources are supplied as one initial pulse and then are depleted until growth stops (for an analogous case in chemostat cultures, see Fig. S8). The shape of these trajectories is dictated by the intrinsic yield Y_i of each resource i (Methods and Supplementary Information Sec. S8); in simple terms this is the amount of new biomass produced per unit of that resource. If the intrinsic yields are constant, then these trajectories are straight lines (Fig. 4A, green line; Supplementary Information Sec. S8) and the slope is the ratio of the intrinsic yields (Supplementary Information Sec. S8). On the other hand, if the intrinsic yields vary over the growth cycle — for example, because they depend on the external resource concentrations which change over time — then the resource depletion trajectories can curve (Fig. 4A, orange line; see also Fig. S9). Possible mechanisms for dynamic intrinsic yields include changes in maintenance resource requirements to maintain existing biomass (Supplementary Information Sec. S9) or growth rate-regulated proteome allocation (Supplementary Information Sec. S10).

Biomass production might stop only when one or more resources reaches zero concentration (vertical and horizontal gray dashed lines in Fig. 4A, with resource trajectories stopping at the green and orange squares). However, in practice biomass production often stops at some nonzero resource concentrations (curved gray dashed line in Fig. 4A, with resource trajectories stopping at the green and orange crosses). The idea is conceptually similar to the experimentally defined R^* value [29]. It is possible for resource thresholds to depend on each other, for instance if death rates scale with growth, or if maintenence resource requirements are dynamically regulated (Supplementary Information Sec. S8; see also Fig. S10).

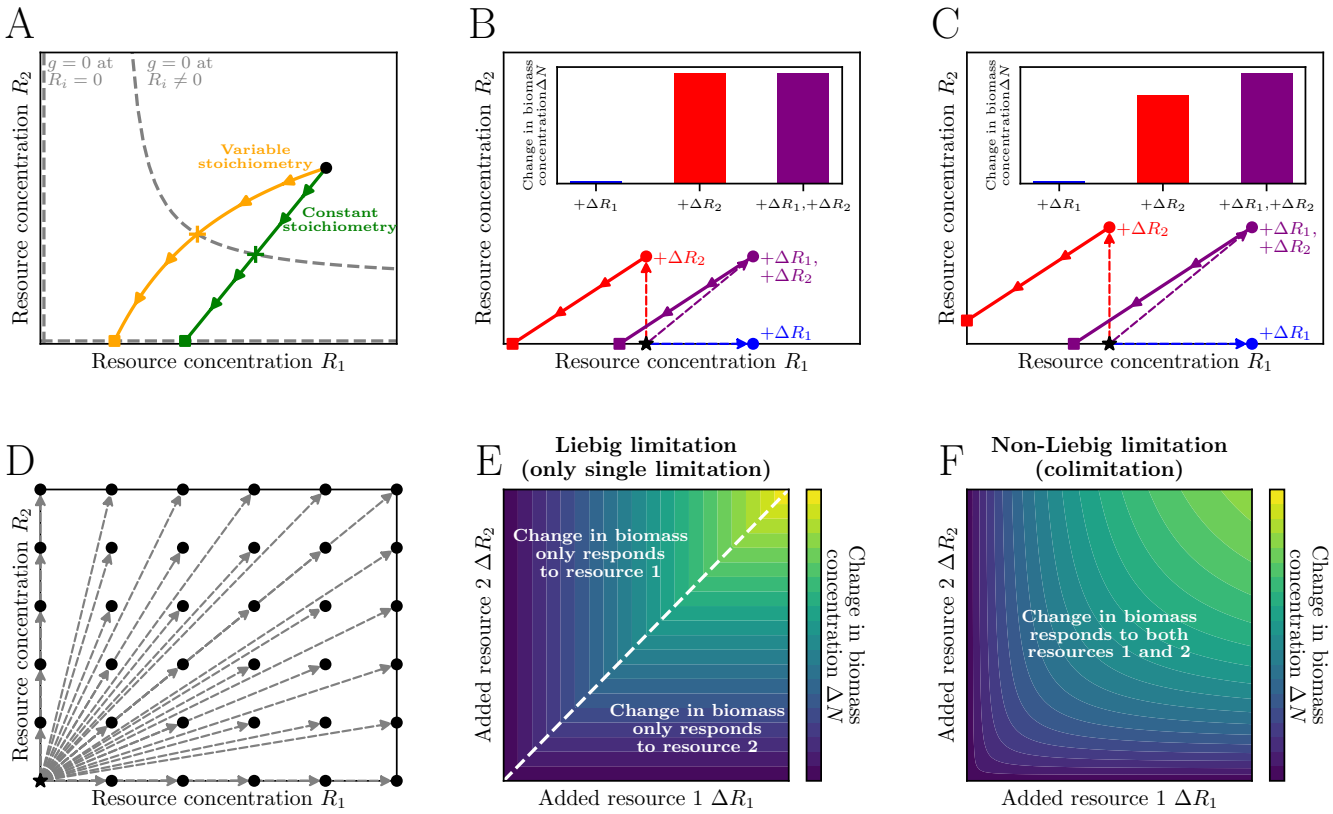

FIG. 4. **Depletion dynamics of resources and concepts of yield limitation and colimitation.** (A) Schematic depletion dynamics for two resources over a batch culture growth cycle. The trajectory of resource concentrations under constant stoichiometry (green line with arrows) must be straight (Supplementary Information Sec. S8), while the trajectory can curve (orange line with arrows) if stoichiometry is variable. Squares mark potential endpoints of the trajectories if growth only stops when at least one resource is completed depleted (vertical and horizontal gray dashed lines), and crosses mark potential endpoints if growth stops at a nonzero combination of resource concentrations (curved gray dashed line). (B) Schematic of a resource supplementation experiment in the space of two resource concentrations. The biomass starts at the black star where it is no longer growing (due to depletion of resource 2). We then supplement either resource 1 (dashed blue line), resource 2 (dashed red line), or both (dashed purple line). The resource depletion trajectories that follow are shown as solid lines with arrows, starting from the dots and ending at the squares. In the inset, we show the amount of additional biomass ΔN produced along each of these trajectories, with colors matching the different supplementations. (See Fig. S11 for an example with a non-Liebig model.) (C) Same as (B) but with larger amounts of supplemented resources. (D) Schematic of a systematic scan of resource supplements, where we start from a population depleted for both resources (at the black star) and systematically add many different combinations of both resources (dashed gray lines). We then track biomass growth starting from each black star and plot how that new biomass amount varies with the amounts of the supplemented resources. (E) Example of biomass production as a function of two supplemented resources, resulting from the setup in (D). The white dashed lines partitions supplementation conditions into a set of conditions where the change in biomass only responds to supplementing one resource or the other, but not both. This is therefore an example of Liebig limitation for biomass (Eq. 6, Supplementary Information Sec. S8). (F) Same as (E) but with non-Liebig biomass limitation, where biomass production depends on both supplemented resources simultaneously.

Biomass yield limitation is the response to a perturbation in resource supply. How do we define limitation of biomass yield? Intuitively, we could consider which nutrient reaches zero concentration by the end of growth (i.e., which axis the depletion trajectory hits first in Fig. 4A) [27]. However, this chemical definition masks the fact that nutrient limitation is a biological phenomenon. The chemical definition may also be impractical, because it is often not possible to empirically determine if a resource is completely exhausted in an environment, and because growth may stop before this point.

Alternatively, we can measure the response of biomass production to a perturbation in the resource supply and define limitation from the biological response. This approach is commonly used in field studies in the aquatic sciences [15, 18–20, 41]. Figure 4B illustrates a typical scenario for this: we start with a population in a state of zero growth, supplement each resource i by some amount ΔR_i, and measure how much biomass grows

after a growth cycle. In Fig. 4B, we see that supplementing resource 1 (dashed blue arrow) leads to no additional biomass (inset, blue bar), while supplementing resource 2 (dashed red arrow) leads to significant additional biomass (inset, red bar); we could interpret this as showing that resource 2 is limiting biomass production. To detect colimitation, we can supplement both resources together (Fig. 4B, dashed purple arrow) and see how much additional biomass grows; in this example, the same amount of biomass grows with the double supplement compared to supplementing resource 2 alone, suggesting the biomass yield is only under single limitation for resource 2.

This factorial approach can be difficult to interpret when the starting condition of the experiment is concealed. This is because the outcome clearly depends on the amounts of each resource that we choose to supplement. Figure 4C shows a similar supplementation experiment, but where the amounts of added resources are greater than in Fig. 4B. In this case, adding resource 1 alone has no effect, but adding it in combination with resource 2 produces a greater amount of biomass than adding resource 2 alone. The reason is that the perturbation has switched the identity of the resource that gets ultimately exhausted. The problem is evident even in this simple Liebig-minimizing case, and would be exacerbated in situations in which colimitation is occurring (Fig. S11).

One way to constrain nutrient colimitation without prior knowledge of the starting state is to scan a surface of supplementation amounts, rather than focusing on a single factorial supplementation [17]. For instance, in Fig. 4D we start with a population that has zero concentration of both resources, and then we supplement both resources in different amounts and measure the total biomass after a growth cycle. The data is then visualized as a heatmap of added biomass yield (Fig. 4E), rather than a set of bars for each discrete condition (Fig. 4B,C, insets).

The systematic scan of nutrient surfaces allows a quantitative definition of limitation to be applied and interpreted without prior knowledge of the system's starting conditions. We define realized biomass yield limitation for a resource as the relative change in biomass for a relative change in the added resource:

$$L^{\text{yield}} = \frac{R}{N}\frac{\partial N}{\partial R}. \tag{4}$$

We also quantify relative colimitation in terms of the effective number of yield-limiting resources:

$$M_{\text{eff}}^{\text{yield}} = \frac{\sum_{\text{resource } i} L_i^{\text{yield}}}{\max_{\text{resource } i} L_i^{\text{yield}}}. \tag{5}$$

Biomass yield limitation is not equivalent to growth rate limitation. Mathematically, the limitation metrics for growth rate (Eqs. 2 and 3) and biomass yield (Eqs. 4 and 5) are similar. However, they are biologically distinct: the former describes the effect on how *fast* growth occurs, while the latter describes the effect on how *much* growth occurs. Growth rate limitation is an instantaneous property of a population. In contrast, biomass yield limitation is a property of a population realized over a finite time period. A population can experience multiple different growth rate limitation regimes over that time period, and these may or many not match the limitation for biomass yield over the whole time.

The distinction between growth rate and biomass yield is analogous to properties of cars. The maximum speed of a car may be limited by air intake or drag, while the range will be limited by fuel or battery capacity. These variables might interact, but are largely independent of each other. Which of these limitation properties is more important to a system depends on the context. For microbes, growth rate limitation is likely to be more important to evolution, since growth rate is under direct selection while biomass production may not be (depending on spatial structure and privatization of resources [42]). Biomass yield limitation, on the other hand, may be important in situations where we care about environmental and ecological composition, like elemental cycling in the ocean or total production in biotechnology applications [43–45].

Biomass yield colimitation arises from interactions between resources. The classic way to model biomass yield is Liebig's law. In this case, only one resource at a time can have a nonzero limitation coefficient L^{yield}, and thus the number of biomass limiting resources is always $M_{\text{eff}}^{\text{yield}} = 1$. The biomass yield is set by whichever resource is stoichiometrically scarcest (Fig. 4E and Supplementary Information Sec. S8):

$$N = \min_{\text{resource } i} R_i Y_i, \tag{6}$$

where N is the amount of biomass that can be produced, R_i is the resource concentration, and Y_i is the intrinsic yield of the population growing on that resource.

Alternatively, we can consider a non-Liebig case, where biomass responds to small changes in both resources simultaneously (Fig. 4F). Here, all resources have nonzero limitation coefficients L_i^{yield}, and therefore there is nonzero colimitation ($M_{\text{eff}}^{\text{yield}} > 1$). This implies that there are interactions between the resources. Briefly, if the biomass yield on one resource depends on the other resource, or if the concentration of one resource at which growth stops depends on the other resource, then biomass production will depend on both resources simultaneously, and hence the two resources will be colimiting. For further discussion, see Supplementary Information Sec. S8.

Biomass yield colimitation is readily accessible under laboratory conditions. As with growth rate, we can determine conditions under which two resources colimit biomass yield by systematically varying them and measuring biomass production under laboratory condi-

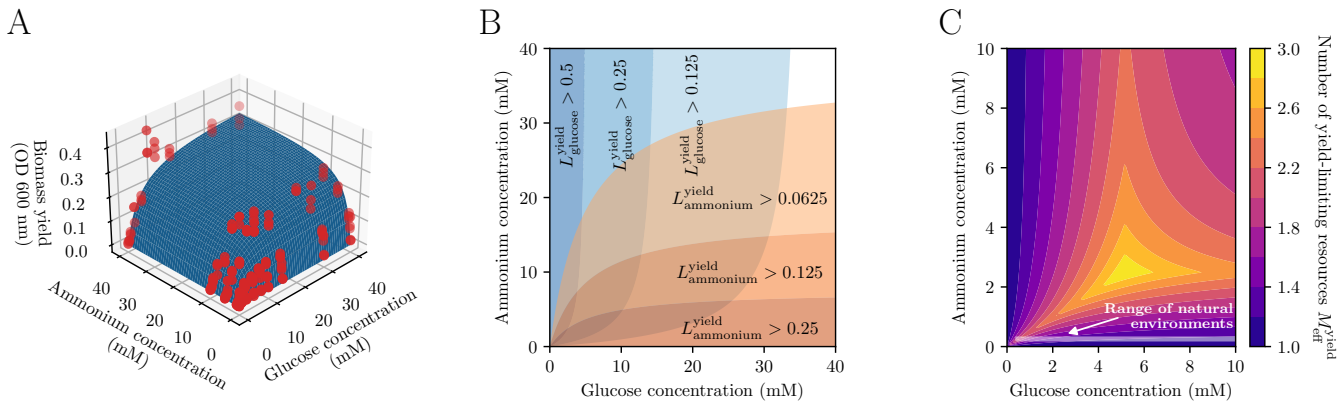

FIG. 5. **Experimental measurements of yield limitation and colimitation.** (A) Biomass measurements (as optical density at 600 nm, red points) over glucose and ammonium concentrations for *E. coli* in minimal medium (Methods, Dataset S3; see Figs. S13 and S14 for growth curves). The blue surface is the best-fit model (generalized-mean model with $N_{\text{fixed}} \approx 0.39$ OD, $Y_{\text{glucose}} \approx 0.076$ OD/mM glucose, $Y_{\text{ammonium}} \approx 0.16$ OD/mM ammonium, $q \approx -1.0$, Eq. 7; Methods and Supplementary Information Sec. S12). (B) Using the model fitted in (A), we calculate regions of yield limitation coefficients L^{yield} (Eq. 4) for glucose (blue) and ammonium (orange) across concentrations. The overlap between these regions indicates conditions where both resources are absolutely colimiting. (C) Using the model fitted in (A), we calculate yield colimitation of glucose and ammonium (number of yield-limiting resources $M^{\text{yield}}_{\text{eff}}$, Eq. 5) across concentrations of both resources. Note that the apparent maximum number of limiting resources is $M^{\text{yield}}_{\text{eff}} = 3$ because of the third, unmeasured resource that becomes limiting for biomass yield when glucose and ammonium are saturated.

tions (Figs. S13 and S14). We take as an example *E. coli* growing in batch conditions with varying initial supply of a carbon source (glucose) and a nitrogen source (ammonium). Figure 5A shows how the total biomass of *E. coli* in batch conditions varies with the initial supply of glucose and ammonium. To determine biomass limitation at these different concentrations, we fit this dependence to a model. We use a phenomenological model of biomass N dependence on resources R_i inspired by the mathematical concept of a generalized mean (Supplementary Information Sec. S12, Fig. S12):

$$N(R_1, R_2, \ldots, R_M) = \left(\sum_{\text{resource } i} (R_i Y_i)^q \right)^{1/q}, \qquad (7)$$

where Y_i is the intrinsic yield per unit of resource i. We interpret the parameter q as quantifying the extent of interaction between resources. In the limit of $q \to -\infty$, this model is equivalent to the Liebig model (Eq. 6; Fig. S12). Finite values of q therefore represent deviations from the Liebig model, implying an interaction between the resources (Supplementary Information Sec. S8). For this reason, we call q the interaction parameter. Finite values of q mean there is some range of conditions where resources colimit biomass yield (Fig. S12). We fit this model to our data and it matches closely (Fig. 5A), with a finite q value and a statistically significant improvement over the Liebig model (Fig. S15).

As with growth rate, we can now use the fitted model to quantify biomass yield limitation and colimitation (Fig. 5B,C). Due to hidden constraints, biomass production does not proceed infinitely; this is modeled as an implied unmeasured resource that will eventually limit biomass once the focal resources are sufficiently abundant. Thus, there is a condition where the model predicts three limiting resources. We model this as limitation by a third, hidden nutrient; however, in practice a non-nutrient constraint such as production of a toxin or limitation for physical space could occur. For *E. coli*, biomass yield colimitation is evident in environmentally relevant concentrations (Fig. 5C), suggesting that in nature, *E. coli* biomass production is best understood in the context of multiple nutrients.

Estimating biomass yield limitation and colimitation in natural environments. As with growth rate limitation, we now demonstrate our approach to biomass yield limitation using data from natural environments. We consider elemental resources for phytoplankton in the ocean, using coarse-grained data from Moore et al. [20]. Using the measured elemental composition of phytoplankton, we calculate the biomass yield for the available concentration of each element (Fig. 6A). This shows roughly three tiers of resources, separated by orders of magnitude: the trace metals iron, cobalt, and manganese have the lowest yields, followed by another set of similar yields for nitrogen, phosphorus, and other metals. The remaining elements all have much higher yields.

We calculate limitation coefficients for each resource using the resource concentrations and intrinsic yield (as ratios relative to carbon) reported by Moore et al. [20]. Since we do not know how biomass depends on multiple resources, we use the generalized-mean model (Eq. 7) to make predictions for representative values of the inter-

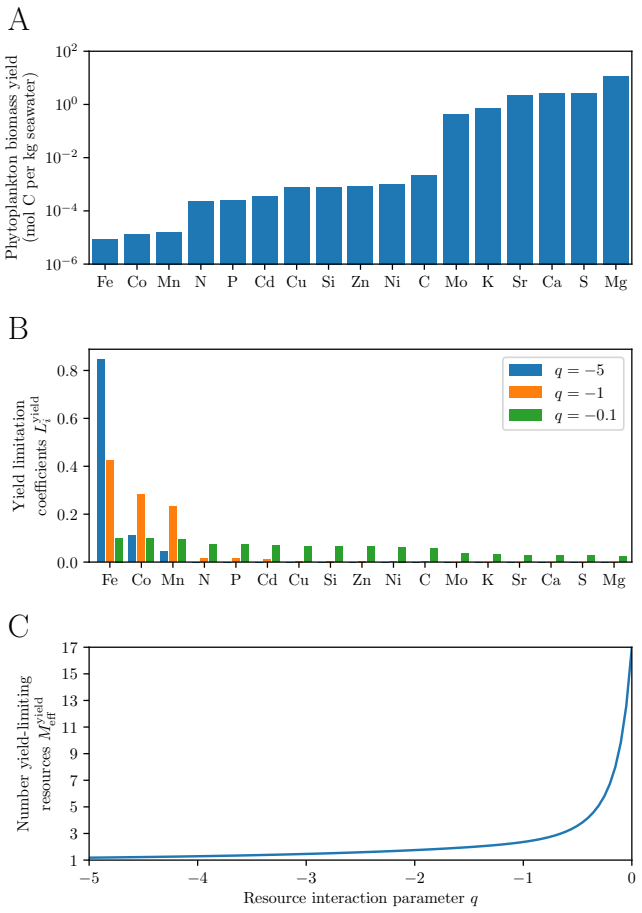

FIG. 6. **Applying yield limitation concepts to empirical data for marine phytoplankton.** (A) Estimated phytoplankton biomass yield per kg of seawater supported by each elemental resource's environmental concentration. Data is from Moore et al. [20]. (B) Using biomass yields from (A), we calculate yield limitation coefficients L^{yield} for each elemental resource. Since we do not know the underlying model for how multiple resources contribute to biomass, we calculate limitation using different values of the resource interaction parameter q (colors) in the generalized-mean model of biomass (Eq. 7, Supplementary Information Sec. S12). (C) Number of yield-limiting resources $M_{\text{eff}}^{\text{yield}}$ as a function of the interaction parameter q, using data from (A).

action parameter q (Fig. 6B). For lower values of q (less interaction), limitation is more strongly concentrated in the resource most rare relative to their biomass requirements, especially iron. This is because this regime is closer to Liebig limitation, where only one resource (the most rare) can be limiting at a time. For higher values of q, we see more equal levels of limitation across resources. Figure 6C quantifies this using the number of biomass limiting resources $M_{\text{eff}}^{\text{yield}}$.

Given that the macronutrients N and P are known to be limiting to marine phytoplankton, it is interesting that N and P limitation are only appreciably limiting in the strong interaction scenarios. While the data we used is coarse-grained and does not account for temporal, spatial, and biological variability (including plasticity in resource use), it does capture overall patterns in resource availability in the surface ocean [20]. The results imply that to determine the true level of colimitation for these populations, we would need to measure the dependence of phytoplankton biomass across many resources simultaneously.

DISCUSSION

Nutrient colimitation occurs when microbial growth is limited by multiple nutrients simultaneously, instead of just by a single most-limiting nutrient. Here we show that nutrient colimitation can be treated quantitatively, and more broadly that nutrient limitation can be thought of as a continuum, both in terms of the degree of absolute limitation (L^{rate} and L^{yield}) and the number of limiting nutrients ($M_{\text{eff}}^{\text{rate}}$ and $M_{\text{eff}}^{\text{yield}}$). This allows us to statistically assess how well different models of growth rate and biomass yield represent real laboratory data. Specifically, we showed that Liebig minimizing functions are not sufficient to explain the growth rate and biomass yields of clonal populations of *E. coli* growing on glucose and ammonium, including in the range of resource concentrations that are found in its natural habitat.

For practical reasons, laboratory experiments usually focus on single nutrient limitations and consider them in discrete, on/off scenarios. However, this lessens what we can comprehend about microbial growth in nature, where colimitation is possible. The metrics L^{rate}, L^{yield}, $M_{\text{eff}}^{\text{rate}}$, and $M_{\text{eff}}^{\text{yield}}$ it possible to make direct, quantitative comparisons between experiments and in situ nutrient conditions and to bridge the gap between the lab and nature. In particular, we highlight that there is added value in sampling two-dimensional "surfaces" of nutrient concentrations, as opposed to single-concentration factorial experiments [17]. This is especially useful when the starting conditions of the system are unknown, as is usually the case in field studies.

We provided a foundational example of a colimited clonal population growing on essential, non-substitutable resources; however, the concepts can be extended to other scenarios such as substitutable resources and colimitation involving direct biochemical interactions between nutrients, such as when a metal cofactor is required for uptake of another nutrient. Our laboratory data indicated that glucose and ammonium interact to determine the growth rates and biomass production yields of *E. coli* populations.

What could be the mechanisms of colimitation for essential nutrients? Intuitively, colimitation implies a physiological tradeoff due to constraints on molecular composition, nutrient uptake, or energy utilization that is exacerbated when multiple resources are rare. This could manifest in stoichiometric flexibility, which may be a direct result of growth optimization in nutrient colimited

conditions [36].

There are also environmental drivers. In aquatic systems with low nutrient concentrations, microscale environmental heterogeneity can reduce the chance that cells encounter both necessary resources quickly; this is implicit in the Poisson Arrival Time (PAT) model that we have considered [46]. A combination of micro- and macro-scale biogeochemical cycling implies that nutrients co-vary in predictable ways; organisms could take advantage of this and regulate their growth in response to multiple nutrients. Phenotypic heterogeneity within the population can also occur [47] and would be relevant if a subset of the population is primarily limited for resource 1 while another subset is limited for resource 2. Lastly, and most broadly, we expect that the requirements of microbial life and the elemental composition of their surroundings coevolve with one another and that this may increase the possibility for nutrient colimitation in nature [48, 49].

In nature, colimitation of clonal populations is also layered with community colimitation, for instance, when members of the community have different nutrient preferences [31, 32]. In this case, the starting conditions of the system are even less clear than for clonal populations, and supplementation experiments that scan a surface of nutrient concentrations in multiple dimensions provide a critical advantage for quantifying the extent of limitation and the number of limiting resources. Also useful are calibrated molecular biomarkers for different nutrient limitations, because these avoid experimental effects in laboratory perturbations, and can identify how strain and even sub-strain level nutrient limitations vary in the community [50, 51]. If nutrient colimitation represents a distinct physiological state for a population or community, it is possible that specific biomarkers for nutrient colimitation can also be identified.

Nutrient colimitation of microbial populations and communities may be a common state of nature, instead of a special case. It is a sensible outcome of eco-evolutionary theory and biogeochemistry and has been observed in a variety of natural habitats [22]. As we have shown, careful experimental design, including testing for colimitation across 2D resource ranges, enhances the chance to observe colimitation and identify colimitation conditions for further experimentation. Quantitative metrics of limitation and colimitation will facilitate laboratory experimentation of the underlying biochemical, molecular, systems biology, and ecological mechanisms. This is important because as examples in *E. coli* and in nature have shown, colimitation is possible and even likely in the natural resource conditions in which organisms evolve. This context is critical for understanding even the most fundamental properties of cells, can help us to better predict, manage, and exploit the growth of microbes, and underscores the connectivity between microbial life and the environment.

METHODS

Numerical methods. We performed all numerical calculations in Python version 3.10.9, using tools from NumPy [52] version 1.24.1 and SciPy [53] version 1.10.0. We prepared all figures using Matplotlib [54] version 3.7.1.

Model of batch growth. Throughout the main text we focus on microbial growth under batch conditions, meaning an initial biomass is given a fixed supply of resources, which it consumes until growth stops. Let $N(t)$ be the concentration of biomass and $\mathbf{R}(t) = (R_1(t), R_2(t), \ldots, R_M(t))$ the vector of all M resource concentrations in the environment at time t, with some fixed initial conditions $N(0)$ and $\mathbf{R}(0)$. Their dynamics over time are determined by

$$\begin{aligned} \frac{d}{dt}N(t) &= g(\mathbf{R}(t))N(t), \\ \frac{d}{dt}R_i(t) &= -\frac{1}{Y_i}\frac{d}{dt}N(t), \end{aligned} \tag{8}$$

where $g(\mathbf{R})$ is the per-capita biomass growth rate that depends on the environmental resource concentrations and Y_i is the intrinsic yield (amount of new biomass produced per unit resource, with all other resource unlimited) for resource i. We solve these equations numerically using `scipy.integrate.solve_ivp` (e.g., Fig. 1D).

Summary of growth rate models. We focus on four widely-used models of how growth rate depends on multiple resources. In the case of two resources, these models are

$$\begin{aligned} \text{Liebig model [15, 28, 34]: } g(R_1,R_2) &= \min\left(\frac{g_{\max,1}R_1}{R_1+K_1}, \frac{g_{\max,2}R_2}{R_2+K_2}\right), \\ \text{Poisson arrival time (PAT) model [2, 34]: } g(R_1,R_2) &= g_{\max}\frac{\frac{R_1}{K_1}\frac{R_2}{K_2}\left(\frac{R_1}{K_1}+\frac{R_2}{K_2}\right)}{\frac{R_1}{K_1}\frac{R_2}{K_2}\left(\frac{R_1}{K_1}+\frac{R_2}{K_2}\right)+\left(\frac{R_1}{K_1}\right)^2+\frac{R_1}{K_1}\frac{R_2}{K_2}+\left(\frac{R_2}{K_2}\right)^2}, \\ \text{Additive model [2, 34]: } g(R_1,R_2) &= g_{\max}\frac{\frac{R_1}{K_1}\frac{R_2}{K_2}}{\frac{R_1}{K_1}\frac{R_2}{K_2}+\frac{R_1}{K_1}+\frac{R_2}{K_2}}, \\ \text{Multiplicative model [2, 28]: } g(R_1,R_2) &= g_{\max}\left(\frac{R_1}{R_1+K_1}\right)\left(\frac{R_2}{R_2+K_2}\right), \end{aligned} \tag{9}$$

where $g_{\max}$ is the maximum possible growth rate and K_i is the half-saturation concentration for resource i. Supplementary Information Sec. S4 contains complete details of these models, including generalizations of these models to an arbitrary number of resources and some heuristic derivations.

Experimental measurement of bacterial growth curves. To profile the growth of bacteria in nutrient colimitation, we used the strain *Escherichia coli* sp. MG1655 pCS-λ [55], which contains a luciferase protein expressed from the constitutive Lambda CS promoter under kanamycin selection. We selected single clones and grew overnight cultures in modified M9 minimal medium. This medium base was composed of a modified M9 salt base without nitrogen (for 1 L of 5X concentrated M9 salt base without nitrogen: 64 g $Na_2HPO_4 \cdot 7H_2O$ (Sigma Aldrich BioXtra grade lot SLBV4967, CAS S9390-500G), 15 g KH_2PO_4 monobasic (Sigma Aldrich ACS grade lot SZBF350AV CAS P0062-500G), and 2.5 g NaCl (Sigma Aldrich BioXtra grade lot SYBG1530V CAS S7653-250G)). We also added 500 mM $MgSO_4$ hexahydrate (Sigma Aldrich ACS grade Lot BCBT5460) and 50 μg/mL kanamycin (Sigma Aldrich CAS 70560-51-9 Lot 0000130025). For overnight cultures, we added 20 mM ammonium chloride (Sigma Aldrich ACS Reagent Lot STBH3180 CAS 31107-500G) and 10 mM D(+)glucose (Sigma Aldrich BioXtra grade Lot SLBW5196 CAS G7528-1Kg); previous experiments indicated that this combination provides for nutrient replete growth with ultimate biomass yield limitation by glucose.

After growing into stationary phase overnight, we collected the cells by centrifugation and washed three times in the modified 1X M9 salts without nitrogen, then adjusted to OD 0.01 in the modified 1X M9 salts without nitrogen. We inoculated the cells in a 1:10 ratio resulting in a final OD of 0.001 into the wells of white walled, flat base 96 well plates (Corning) containing the 1X modified M9 medium without nitrogen and pre-defined combinations of ammonium chloride and D-glucose, which were added from concentrated stocks prepared in the 1X modified M9 salt without nitrogen base. For the scan of growth rate, we varied ammonium between 0 and 1 mM and glucose between 0 and 2 mM. We monitored luminescence across triplicate plates, measured simultaneously using three plate readers from the same manufacturer (Biotek Synergy H1) with similar settings implemented (37 C, orbital shaking of 15 s prior to each measurement, luminescence integration time of 3 s). For the scan of biomass yield, we varied ammonium between 0 and 40 mM and glucose between 0 and 150 mM. In that case we monitored growth as optical density at 600 nm using the Tecan Infinite plate reader connected to the Tecan Freedom Evo robotic system. Raw growth curve data is in Datasets S1 and S3.

Analysis of growth curve data for growth rates and biomass yield. We analyzed growth curves using the open source AMiGA library [56]. In the growth rate data, we observed an initial spike in luminescence at the immediate start of the experiment due to acclimation or possible condensation, so we truncated the first six data points prior to AMiGA fitting. We did not use any truncation for the biomass yield data from OD. We verified growth properties fitted by AMiGA by visually comparing them to the growth curves (Figs. S5, S6, S14, and S14). The fitted growth rates and yields are in Datasets S1 and S3.

We then fit growth rates and biomass yields to models using `scipy.optimize.curve_fit` for least-squares minimization, which reports optimal parameter values and their estimated standard deviations. For the yield scans with replicate measurements, we also estimated uncertainties on fits by bootstrapping 100 simulating data sets from these parameters. We did this by randomly sampling (with replacement) three yields from the three replicate measurements at each initial glucose and ammonium concentration combination. We calculated the Akaike information criterion (corrected for small sample size) for each model fit using

$$\mathrm{AIC} = 2n + n\log\left(\frac{\sum_{i=1}^{n}(f_i - y_i)^2}{n-k}\right) - 2k\left(\frac{k+1}{n-k-1}\right), \quad (10)$$

where n is the number of data points, y_i is the ith measured data point, f_i is the fitted value for that data point, and k is the number of parameters in the model [57]. We calculate the relative Akaike weight for a model α as

$$w_\alpha = \frac{e^{-\frac{1}{2}\mathrm{AIC}_\alpha}}{\sum_{\mathrm{model}\,\beta} e^{-\frac{1}{2}\mathrm{AIC}_\beta}}. \quad (11)$$

Data collection for growth response traits and environmental resource concentrations. We collected 20 studies in which the parameters of the Monod growth model ($g_{\max}$ and K) for two resoures were measured for the same species/strain. We extracted this data from a broader literature review of Monod parameters that we conducted earlier [37]. Whenever possible, we estimated background environmental nutrient concentrations (i.e., the concentrations the organism is expected to experience in the environment from which it was isolated) from data provided in the original manuscript. When this was not provided, we estimated a range of environmental concentrations from the expected habitat of the organism. For instance, for *E. coli* sp. K12, we selected representative environmental concentrations of resources in the human gut (higher concentrations) and in soils (lower concentrations). For marine diatoms, we selected representative environmental concentrations of high nutrient regions (coastal upwelling zones) and low nutrient regions (surface open ocean). In some cases, the expected resource concentration range is large and spans

at least an order of magnitude. For calculations, the mean value of this range was used. Using the measured Monod parameters and estimated environmental concentrations, we calculated limitation coefficients using four common models (Liebig, poisson arrival time model, additive model, and multiplicative model).

ACKNOWLEDGMENTS

NAH was supported by the Principles of Microbial Ecosystems collaboration of the Simons Foundation (grant ID 542379) and an ETH Zurich Career Seed Grant (SEED-26 21-2). MM was supported by an Ambizione grant from the Swiss National Science Foundation (PZ00P3_180147).

[1] James J. Elser, Dean R. Dobberfuhl, Neil A. MacKay, and John H. Schampel. Organism Size, Life History, and N:P Stoichiometry: Toward a unified view of cellular and ecosystem processes. *BioScience*, 46(9):674–684, October 1996.

[2] E. Sperfeld, D. Martin-Creuzburg, and A. Wacker. Multiple resource limitation theory applied to herbivorous consumers: Liebig's minimum rule vs. interactive co-limitation. *Ecol Lett*, 15:142–150, 2012.

[3] Joel E. Cohen. Population Growth and Earth's Human Carrying Capacity. https://www.science.org/doi/10.1126/science.7618100, 1995.

[4] H.J.W. De Baar. Von Liebig's law of the minimum and plankton ecology (1899–1991). *Progress in Oceanography*, 33(4):347–386, January 1994.

[5] Emily J. Zakem and Naomi M. Levine. Systematic Variation in Marine Dissolved Organic Matter Stoichiometry and Remineralization Ratios as a Function of Lability. *Global Biogeochemical Cycles*, 33(11):1389–1407, 2019.

[6] Michael J Follows, Stephanie Dutkiewicz, Scott Grant, and Sallie W Chisholm. Emergent biogeography of microbial communities in a model ocean. *Science (New York, N.Y.)*, 315(5820):1843–6, March 2007.

[7] Michael J Follows and Stephanie Dutkiewicz. Modeling diverse communities of marine microbes. *Annual review of marine science*, 3:427–451, 2011.

[8] Nicolas Gruber, Charles D. Keeling, and Nicholas R. Bates. Interannual Variability in the North Atlantic Ocean Carbon Sink. *Science*, 298(5602):2374–2378, 2002.

[9] Sophia Hsin-Jung Li, Zhiyuan Li, Junyoung O. Park, Christopher G. King, Joshua D. Rabinowitz, Ned S. Wingreen, and Zemer Gitai. Escherichia coli translation strategies differ across carbon, nitrogen and phosphorus limitation conditions. *Nature Microbiology*, 3(8):939–947, August 2018.

[10] Prasad Gyaneshwar, Oleg Paliy, Jon McAuliffe, David L. Popham, Michael I. Jordan, and Sydney Kustu. Sulfur and Nitrogen Limitation in Escherichia coli K-12: Specific Homeostatic Responses. *Journal of Bacteriology*, 187(3):1074–1090, February 2005.

[11] Larry Reitzer. Nitrogen assimilation and global regulation in Escherichia coli. *Annual Review of Microbiology*, 57:155–176, 2003.

[12] Daniel R. Brown, Geraint Barton, Zhensheng Pan, Martin Buck, and Sivaramesh Wigneshweraraj. Nitrogen stress response and stringent response are coupled in Escherichia coli. *Nature Communications*, 5(May):1–8, 2014.

[13] Daniel P. Zimmer, Eric Soupene, Haidy L. Lee, Volker F. Wendisch, Arkady B. Khodursky, Brian J. Peter, Robert A. Bender, and Sydney Kustu. Nitrogen regulatory protein C-controlled genes of Escherichia coli: Scavenging as a defense against nitrogen limitation. *Proceedings of the National Academy of Sciences*, 97(26):14674–14679, December 2000.

[14] M. Danger, C. Oumarou, D. Benest, and G. Lacroix. Bacteria can control stoichiometry and nutrient limitation of phytoplankton. *Functional Ecology*, 21(2):202–210, 2007.

[15] M. A. Saito, T. J. Goepfert, and J. T. Ritt. Some thoughts on the concept of colimitation: Three definitions and the importance of bioavailability. *Limnol Oceanogr*, 53:276–290, 2008.

[16] W. Stanley Harpole, Jacqueline T. Ngai, Elsa E. Cleland, Eric W. Seabloom, Elizabeth T. Borer, Matthew E.S. Bracken, James J. Elser, Daniel S. Gruner, Helmut Hillebrand, Jonathan B. Shurin, and Jennifer E. Smith. Nutrient co-limitation of primary producer communities. *Ecology Letters*, 14(9):852–862, 2011.

[17] Erik Sperfeld, David Raubenheimer, and Alexander Wacker. Bridging factorial and gradient concepts of resource co-limitation: Towards a general framework applied to consumers. *Ecology Letters*, 19(2):201–215, 2016.

[18] Thomas J Browning, P Eric, Insa Rapp, Anja Engel, Erin M Bertrand, Alessandro Tagliabue, and C Mark Moore. Nutrient co-limitation at the boundary of an oceanic gyre. *Nature Publishing Group*, 12, 2017.

[19] James J. Elser, Matthew E.S. Bracken, Elsa E. Cleland, Daniel S. Gruner, W. Stanley Harpole, Helmut Hillebrand, Jacqueline T. Ngai, Eric W. Seabloom, Jonathan B. Shurin, and Jennifer E. Smith. Global analysis of nitrogen and phosphorus limitation of primary producers in freshwater, marine and terrestrial ecosystems. *Ecology Letters*, 10(12):1135–1142, 2007.

[20] C. M. Moore, M. M. Mills, K. R. Arrigo, I. Berman-Frank, L. Bopp, P. W. Boyd, E. D. Galbraith, R. J. Geider, C. Guieu, S. L. Jaccard, T. D. Jickells, J. La Roche, T. M. Lenton, N. M. Mahowald, E. Marañón, I. Marinov, J. K. Moore, T. Nakatsuka, A. Oschlies, M. A. Saito, T. F. Thingstad, A. Tsuda, and O. Ulloa. Processes and Patterns of Oceanic Nutrient Limitation. *Nat Geoscience*, 6:701–710, 2013.

[21] Kevin R Arrigo. Marine microorganisms and global nutrient cycles. *Nature*, 437(September):349–356, 2005.

[22] Thomas J. Browning and C. Mark Moore. Global analysis of ocean phytoplankton nutrient limitation reveals high prevalence of co-limitation. *Nature Communications*, 14(1):5014, August 2023.

[23] Thomas J. Browning, Eric P. Achterberg, Anja Engel, and Edward Mawji. Manganese co-limitation of phytoplankton growth and major nutrient drawdown in the Southern Ocean. *Nature Communications*, 12(1):884, February 2021.

[24] Benjamin S. Twining, Sara Rauschenberg, Steven E. Baer, Michael W. Lomas, Adam C. Martiny, and Olga Antipova. A nutrient limitation mosaic in the eastern tropical Indian Ocean. *Deep Sea Research Part II: Topical Studies in Oceanography*, 166:125–140, August 2019.

[25] Erin M. Bertrand, Mak a. Saito, Julie M. Rose, Christina R. Riesselman, Maeve C. Lohan, Abigail E. Noble, Peter a. Lee, and Giacomo R. DiTullio. Vitamin B12 and iron colimitation of phytoplankton growth in the Ross Sea. *Limnology and Oceanography*, 52(3):1079–1093, 2007.

[26] J. Keith Moore and Scott C. Doney. Iron availability limits the ocean nitrogen inventory stabilizing feedbacks between marine denitrification and nitrogen fixation. *Global Biogeochemical Cycles*, 21(2):1–12, 2007.

[27] Thomas Egli and Manfred Zinn. The concept of multiple-nutrient-limited growth of microorganisms and its application in biotechnological processes. *Biotechnology Advances*, 22(1-2):35–43, 2003.

[28] M. Zinn, B. Witholt, and T. Egli. Dual nutrient limited growth: Models, experimental observations, and applications. *J Biotechnol*, 113:263–279, 2004.

[29] D. Tilman. Tests of Resource Competition Theory Using Four Species of Lake Michigan Algae. *Ecology*, 62(3):802–815, 1981.

[30] David Tilman. THE RESOURCE-RATIO HYPOTHESIS OF PLANT SUCCESSION. *The American Naturalist*, 125(6):827–852, 1985.

[31] Catherine Bannon, Insa Rapp, and Erin M. Bertrand. Community Interaction Co-limitation: Nutrient Limitation in a Marine Microbial Community Context. *Frontiers in Microbiology*, 13, 2022.

[32] Michael Danger, Tanguy Daufresne, Françoise Lucas, Serge Pissard, and Gérard Lacroix. Does Liebig's law of the minimum scale up from species to communities? *Oikos*, 117(11):1741–1751, 2008.

[33] M.R. Droop. Some thoughts on nutrient limitation in algae. *J. Phycol*, 9:264–272, 1974.

[34] R. V. O'Neill, D. L. DeAngelis, J. J. Pastor, B. J. Jackson, and W. M. Post. Multiple nutrient limitations in ecological models. *Ecol Modelling*, 46:147–163, 1989.

[35] J.-C. Poggiale, M. Baklouti, B. Queguiner, and S. A. L. M. Kooijman. How far details are important in ecosystem modelling: The case of multi-limiting nutrients in phytoplankton–zooplankton interactions. *Phil Trans R Soc B*, 365:3495–3507, 2010.

[36] Kai W. Wirtz and Onur Kerimoglu. Autotrophic Stoichiometry Emerging from Optimality and Variable Colimitation. *Frontiers in Ecology and Evolution*, 4, 2016.

[37] J. W. Fink, N. A. Held, and M. Manhart. Microbial population dynamics decouple growth response from environmental nutrient concentration. *Proc Natl Acad Sci USA*, 120:e2207295120, 2023.

[38] J. Monod. The growth of bacterial cultures. *Annu Rev Microbiol*, 3:371–394, 1949.

[39] R. Heinrich and S. Schuster. *The Regulation of Cellular Systems*. Chapman and Hall, New York, 1996.

[40] Jen Nguyen, Juanita Lara-Gutiérrez, and Roman Stocker. Environmental fluctuations and their effects on microbial communities, populations and individuals. *FEMS Microbiology Reviews*, 45(4):fuaa068, July 2021.

[41] Daniel R. O'Donnell, Paul Wilburn, Eugene A. Silow, Lev Y. Yampolsky, and Elena Litchman. Nitrogen and phosphorus colimitation of phytoplankton in Lake Baikal: Insights from a spatial survey and nutrient enrichment experiments. *Limnology and Oceanography*, 62(4):1383–1392, 2017.

[42] H. Bachmann, M. Fischlechner, I. Rabbers, N. Barfa, F. B. dos Santos, D. Molenaar, and B. Teusink. Availability of Public Goods Shapes the Evolution of Competing Metabolic Strategies. *Proc Natl Acad Sci USA*, 110:14302–14307, 2013.

[43] Paul A. del Giorgio and Jonathan J. Cole. Bacterial Growth Efficiency in Natural Aquatic Systems. *Annual Review of Ecology and Systematics*, 29(1):503–541, 1998.

[44] Casey M. Godwin, Emily A. Whitaker, and James B. Cotner. Growth rate and resource imbalance interactively control biomass stoichiometry and elemental quotas of aquatic bacteria. *Ecology*, 98(3):820–829, 2017.

[45] David A. Lipson. The complex relationship between microbial growth rate and yield and its implications for ecosystem processes. *Frontiers in Microbiology*, 6, 2015.

[46] R. Stocker. Marine Microbes See a Sea of Gradients. *Science*, 338(6107):628–633, 2012.

[47] Frank Schreiber, Sten Littmann, Gaute Lavik, Stéphane Escrig, Anders Meibom, Marcel M.M. Kuypers, and Martin Ackermann. Phenotypic heterogeneity driven by nutrient limitation promotes growth in fluctuating environments. *Nature Microbiology*, 1(6):1–7, 2016.

[48] Megan L. Larsen, Steven W. Wilhelm, and Jay T. Lennon. Nutrient stoichiometry shapes microbial coevolution. *Ecology Letters*, 22(6):1009–1018, 2019.

[49] François M. M. Morel. The co-evolution of phytoplankton and trace element cycles in the oceans. *Geobiology*, 6(3):318–324, 2008.

[50] Mak A Saito, Matthew R McIlvin, Dawn M Moran, Tyler J Goepfert, Giacomo R. DiTullio, Anton F. Post, and Carl H Lamborg. Multiple nutrient stresses at intersecting Pacific Ocean biomes detected by protein biomarkers. *Science (New York, N.Y.)*, 345(6201):1173–7, 2014.

[51] Natalie R. Cohen, Matthew R. McIlvin, Dawn M. Moran, Noelle A. Held, Jaclyn K. Saunders, Nicholas J. Hawco, Michael Brosnahan, Giacomo R. DiTullio, Carl Lamborg, John P. McCrow, Chris L. Dupont, Andrew E. Allen, and Mak A. Saito. Dinoflagellates alter their carbon and nutrient metabolic strategies across environmental gradients in the central Pacific Ocean. *Nature Microbiology*, 2021.

[52] C. R. Harris, K. J. Millman, S. J. van der Walt, R. Gommers, P. Virtanen, D. Cournapeau, E. Wieser, J. Taylor, S. Berg, N. J. Smith, R. Kern, M. Picus, S. Hoyer, M. H. van Kerkwijk, M. Brett, A. Haldane, J. Fernández del Río, M. Wiebe, P. Peterson, P. Gérard-Marchant, K. Sheppard, T. Reddy, W. Weckesser, H. Abbasi, C. Gohlke, and T. E. Oliphant. Array programming with NumPy. *Nature*, 585:357–362, 2020.

[53] P. Virtanen, R. Gommers, T. E. Oliphant, M. Haberland, T. Reddy, D. Cournapeau, E. Burovski, P. Peterson, W. Weckesser, J. Bright, S. J. van der Walt, M. Brett, J. Wilson, K. J. Millman, N. Mayorov, A. R. J. Nelson, E. Jones, R. Kern, E. Larson, C. J. Carey, İ Polat, Y. Feng, E. W. Moore, J. VanderPlas, D. Laxalde, J. Perktold, R. Cimrman, I. Henriksen, E. A. Quintero, C. R. Harris, A. M. Archibald, A. H. Ribeiro, F. Pedregosa, P. van Mulbregt, and SciPy 1.0 Contributors. SciPy 1.0: Fundamental Algorithms for Scientific Computing in Python. *Nature Methods*, 17:261–272, 2020.

[54] J. D. Hunter. Matplotlib: A 2D graphics environment. *Computing in Science & Engineering*, 9:90–95, 2007.

[55] R. Kishony and S. Leibler. Environmental Stresses Can Alleviate the Average Deleterious Effect of Mutations. *J Biol*, 2:14, 2003.

[56] F. S. Midani, J. Collins, and R. A. Britton. AMiGA: Software for automated analysis of microbial growth assays. *mSystems*, 6:e00508–21, 2021.

[57] K. P. Burnham and D. R. Anderson. *Model Selection and Multimodal Inference: A Practical Information-Theoretic Approach*. Springer-Verlag, New York, 2nd edition, 2002.

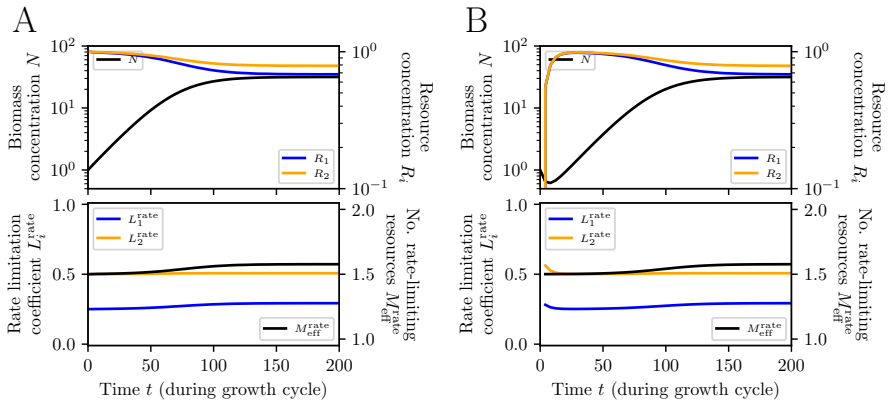

FIG. S1. **Growth and limitation dynamics in continuous (chemostat) cultures.** (A) Simulation of the system shown in Fig. 1C,D but in a chemostat regime, where the resources are supplied at constant rates and the whole system is diluted at a constant rate. The top panel shows the dynamics of biomass (black line) and resource (blue and orange) concentrations over time. The bottom panel shows the rate limitation coefficients $L_i^{\rm rate}$ and the number of rate-limiting resources $M_{\rm eff}^{\rm rate}$ over the same time range. Here the initial condition is such that the resource concentrations in the culture start at equilibrium with the supply concentrations, which the biomass growth then draws down to the steady state (see resource dynamics for the same case in Fig. S8A). (B) Same as (A) but starting with zero resource concentration in the culture (see resource dynamics in Fig. S8B).

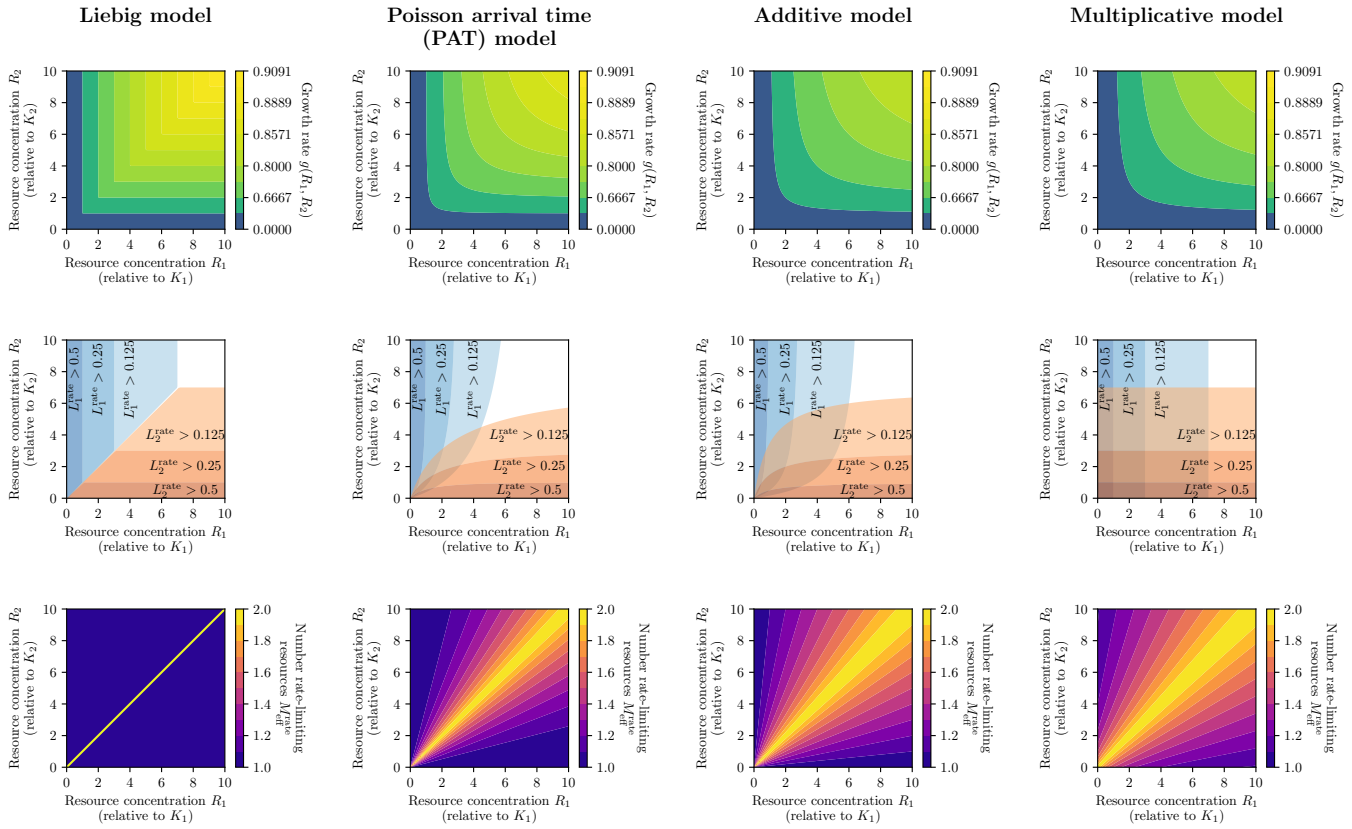

FIG. S2. **Summary of growth rate models and their limitation properties.** Each column corresponds to a different model of how growth rate depends on resource concentrations, as defined in Methods and Supplementary Information Sec. S4. First row: For each growth rate model in a different column, we show the growth rates $g(R_1, R_2)$ as functions of resource concentrations R_1 and R_2. Second row: Rate limitation coefficients for resource 1 ($L_1^{\rm rate}$, blue contours) and for resource 2 ($L_2^{\rm rate}$, orange contours) as functions of resource concentrations (compare to schematic in Fig. 1B). Third row: Number of rate-limiting resources $M_{\rm eff}^{\rm rate}$ (Eq. 3) as functions of resource concentrations. All resource concentrations R_i are scaled relative to their corresponding half-saturation concentrations K_i.

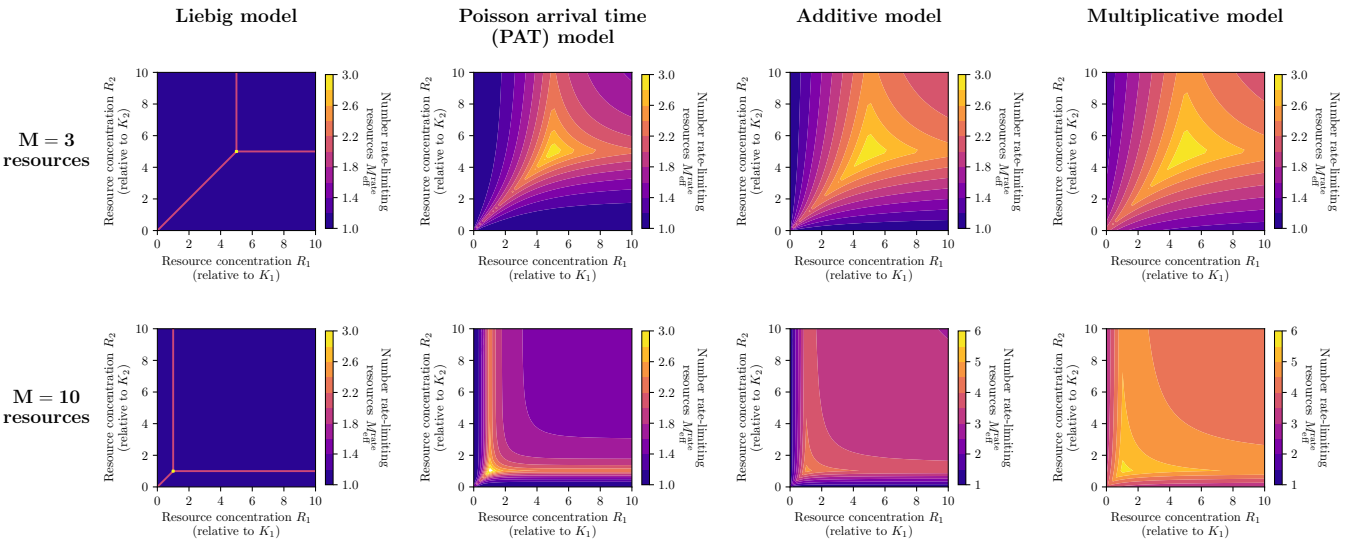

FIG. S3. **Growth rate colimitation with more than two resources.** Each column corresponds to a different model of how growth rate depends on resource concentrations, as defined in Methods and Supplementary Information Sec. S4. First row: Number of rate-limiting resources $M_{\text{eff}}^{\text{rate}}$ (Eq. 3) as functions of resource concentrations R_1 and R_2. Here there are $M = 3$ total resources, with the third resource being held fixed at $R_3/K_3 = 5$, in contrast to Fig. S2 which has similar plots but for only $M = 2$ total resources. The point at which maximum colimitation occurs ($M_{\text{eff}}^{\text{rate}} = 3$) is therefore set by the concentration of this third resource (i.e., where $R_1/K_1 = R_2/K_2 = R_3/K_3$). Second row: Same as the first row but for $M = 10$ total resources, where the additional resources are fixed at $\{R_i/K_i\} = \{5, 1, 2, 3, 4, 5, 6, 7\}$ for $i = 3, 4, \ldots, 10$. The point at which maximum colimitation occurs is set approximately by the most limiting fixed resource (resource 4 with $R_4/K_4 = 1$).

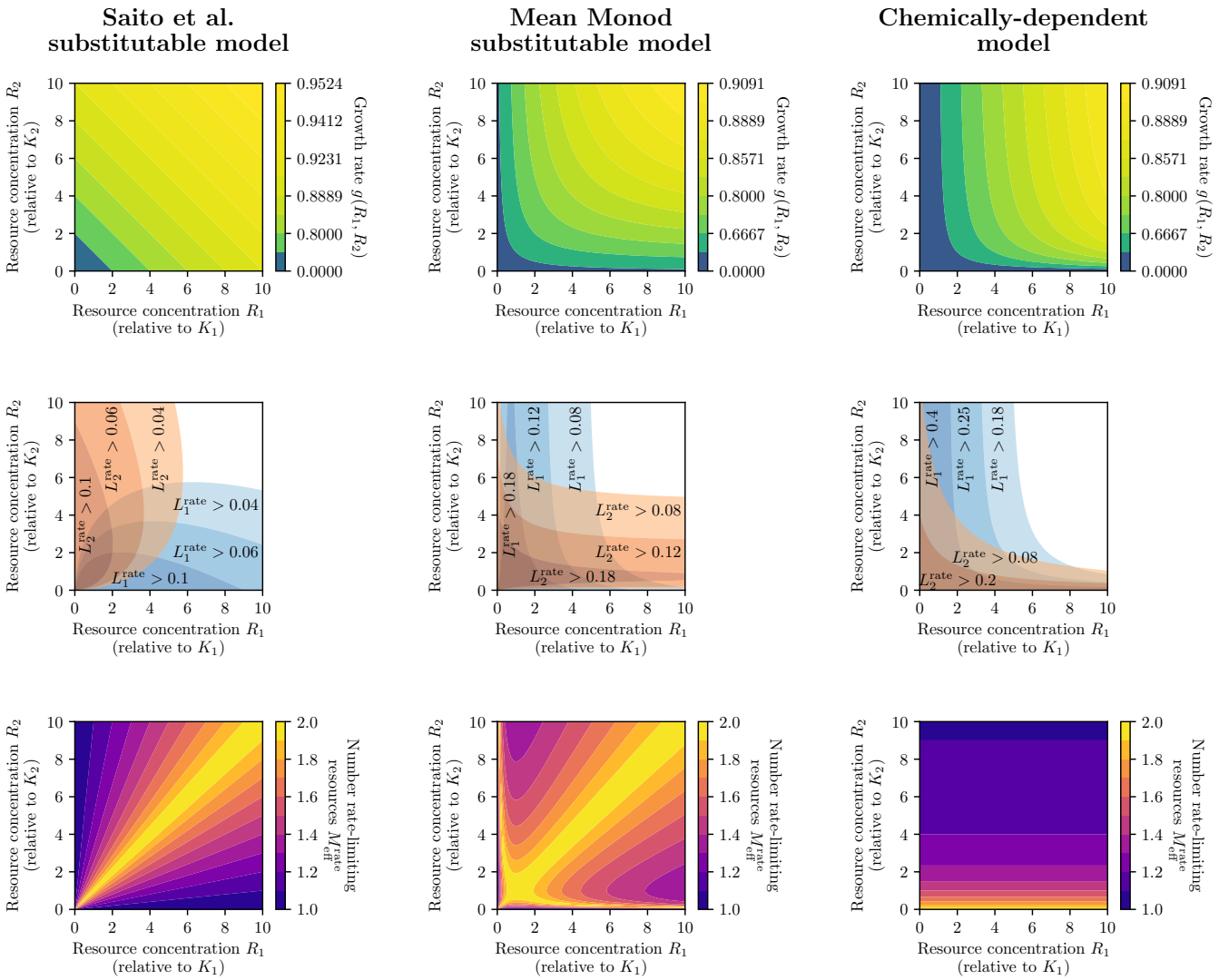

FIG. S4. **Summary of growth rate models and their limitation properties for substitutable and chemically-dependent resources.** Same as Fig. S2 but for the Saito et al. model [15] of substitutable resources (first column), the mean Monod model of substitutable resources (second column), and the model of chemically-dependent resources [15] (third column); see Supplementary Information Secs. S5 and S6 for definitions.

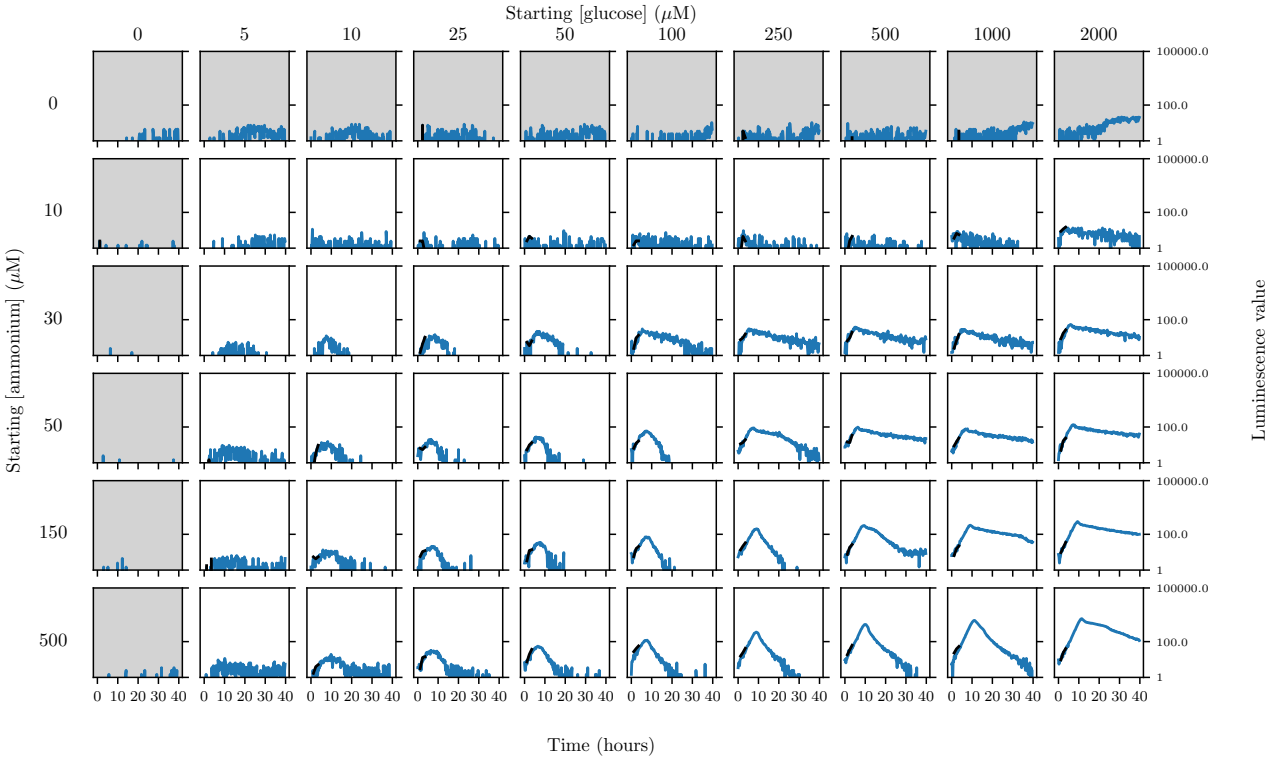

FIG. S5. **Scan of luminescence growth curves across glucose and ammonium concentrations.** Growth curves of luminescent *E. coli* sp. MG1655 pCS-λ [55] with each well having a different starting concentration of glucose and ammonium. The observed maximum growth rates, fitted from the data, are overlayed in black lines. gray shading indicates wells where the concentration of either glucose and/or ammonium was 0 μM.

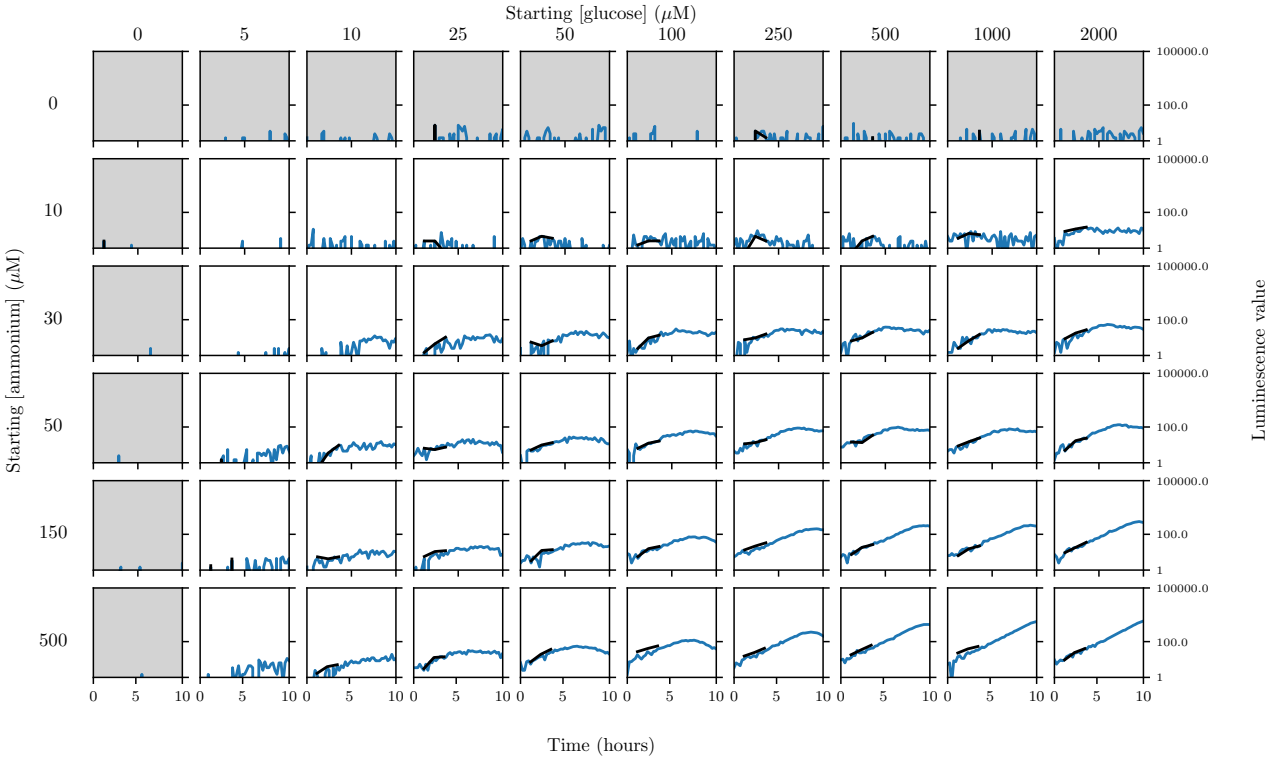

FIG. S6. **Zoomed in view of luminescence growth curves across glucose and ammonium concentrations.** Same as Fig. S5 but zoomed into the first 10 hours.

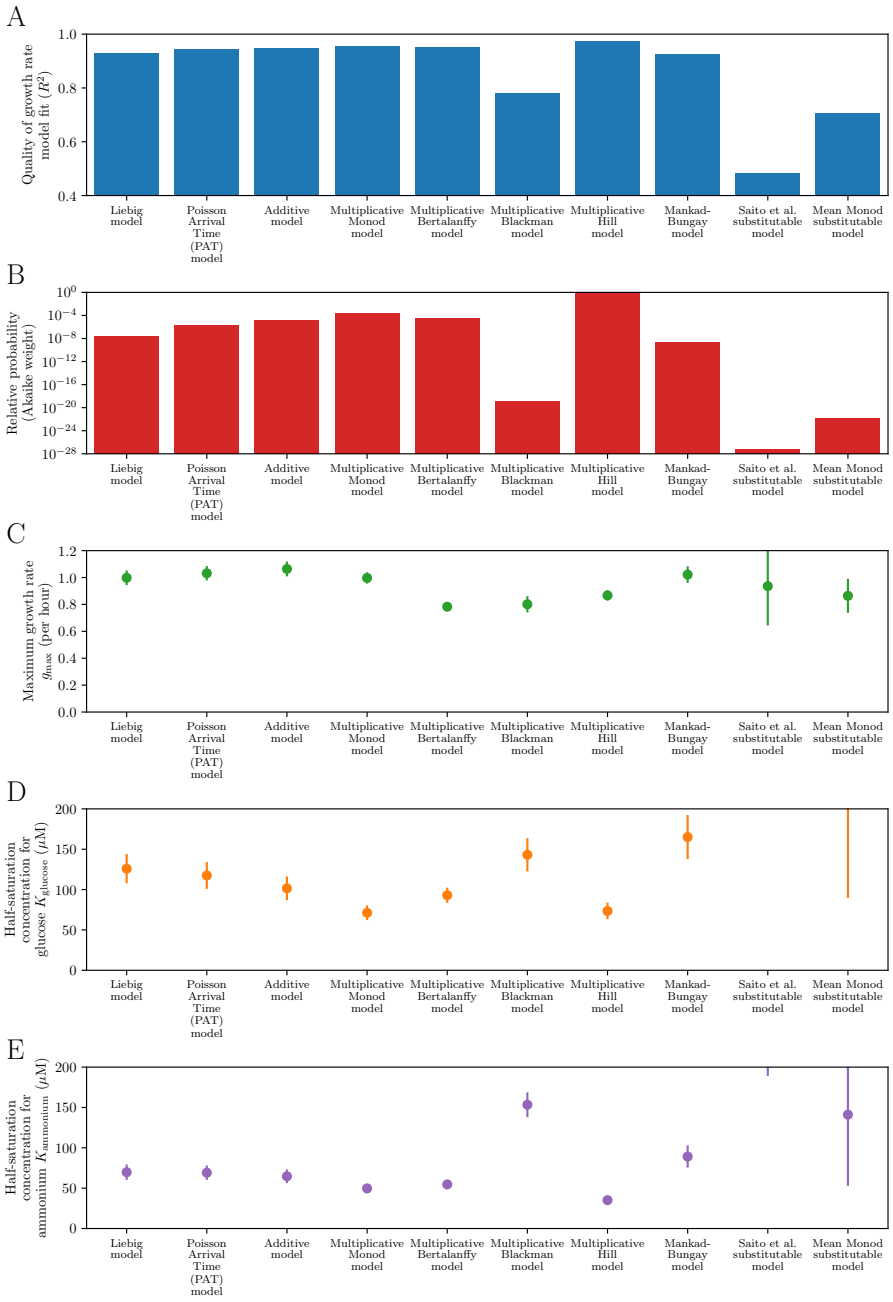

FIG. S7. **Statistics for fitting different growth rate models to experimental data.** We fit several growth rate models (Methods, Supplementary Information Sec. S4) to the population growth rate of *E. coli* as a function of glucose and ammonium concentrations (Figs. 2A, S5, and S6). (A) Quality of fit R^2 for each model. (B) Relative probability of each model fit using its Akaike weight. (C) Value of the maximum growth rate $g_{\max}$ for each fit, with estimated standard deviations shown as vertical bars. (D) Same as (C) but for the fitted half-saturation concentration K_{glucose} for glucose. (D) Same as (C) but for the fitted half-saturation concentration K_{ammonium} for ammonium.

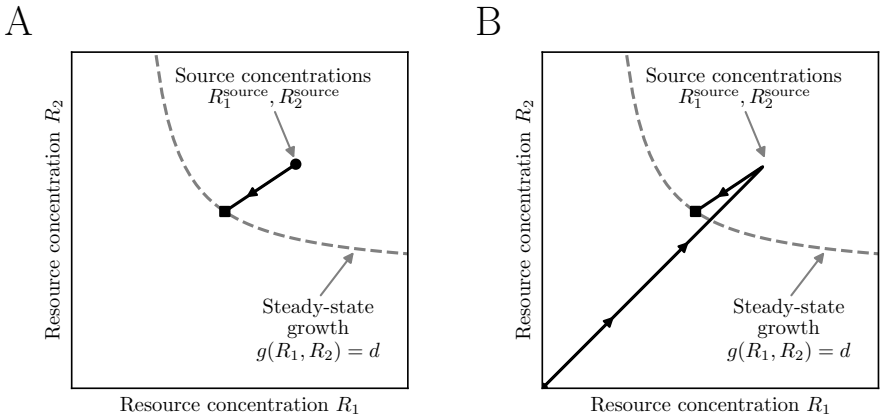

FIG. S8. **Resource dynamics for continuous (chemostat) cultures.** (A) Dynamics of resource concentrations for the same simulation in Fig. S1A. This simulation begins with resources in equilibrium with their source concentrations (black dot), but as the biomass grows, they draw down along a trajectory (black line with arrow) with slope set by their stoichiometry (Supplementary Information Secs. S2 and S8) until they intersect the gray curve (black square) where biomass growth rate equals dilution rate. (B) Same as (A) but for simulation in Fig. S1B, which is the same model but with resources starting at zero concentration in the culture. In this case, the resources initially draw up to reach their source concentrations, but then draw down to the steady state with biomass growth as in (A).

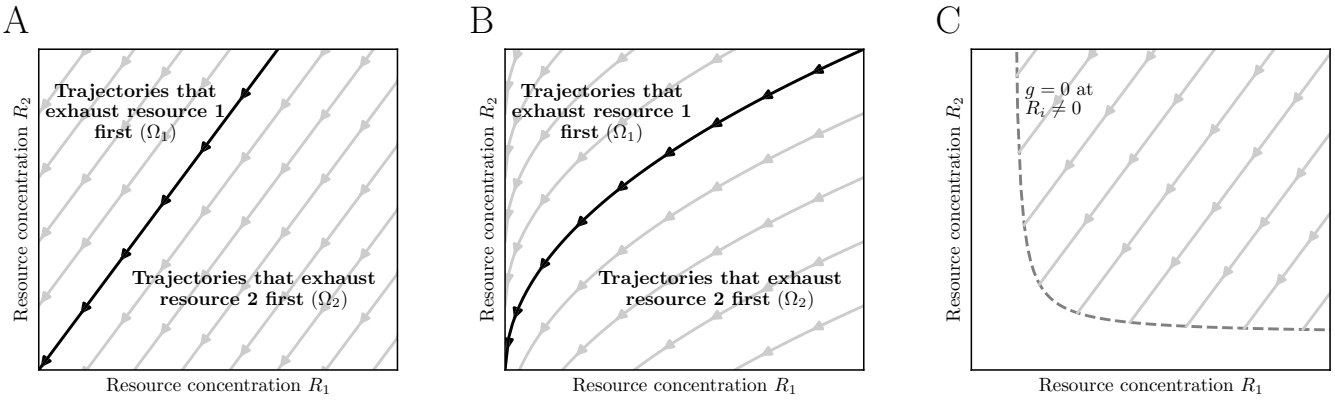

FIG. S9. **Different qualitative regimes of resource depletion trajectories.** (A) If resources are consumed with constant stoichiometry, then their concentrations deplete along straight lines (Supplementary Information Sec. S8). The regions in which the first depleted resource is resource 1 or resource 2 are shown as Ω_1 and Ω_2. (B) Same as (A) but for resources consumed with variable stoichiometry, which causes their depletion trajectories to curve (Supplementary Information Sec. S8). (C) Same as (A) for where resource depletion stops at some nonzero combination of concentrations (dashed gray line), e.g., when growth rate reaches zero.

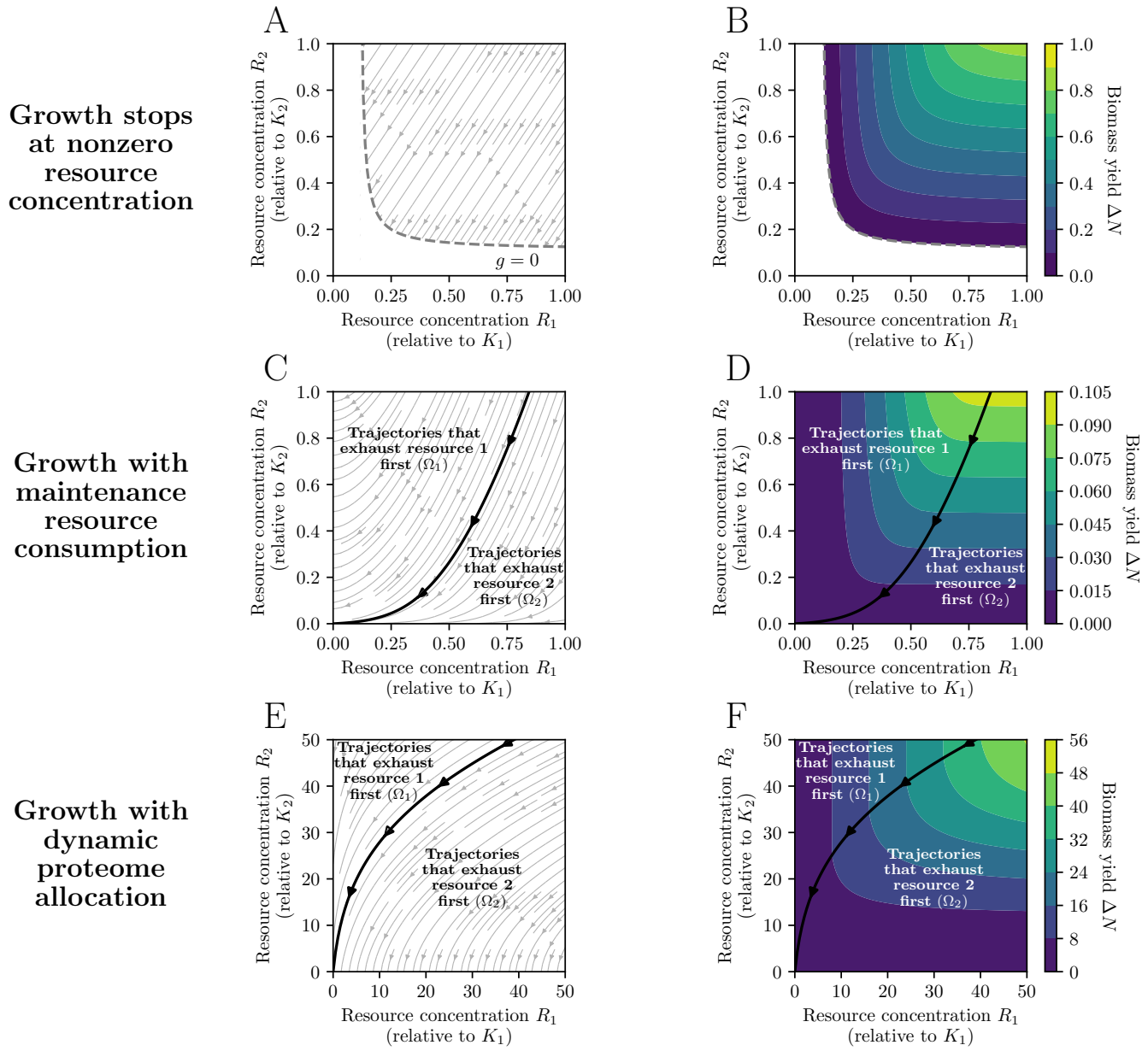

FIG. S10. **Yield limitation in different mechanistic models.** (A) Model of resource consumption in which growth stops at nonzero concentrations of resources (Supplementary Information Sec. S8). These concentrations (Zero Net Growth Isocline, ZNGI) are shown as the dashed gray line in the space of concentrations for resources 1 and 2. Gray stream lines show trajectories of resource depletion with constant stoichiometry. (B) For the model in (A), we calculate the total biomass yield ΔN after one batch growth cycle for all possible initial resource concentrations. (C) Model of resource consumption in which biomass consumes resources for maintenance as well as growth (Supplementary Information Sec. S9). This causes stoichiometry to vary with resource concentration, and so depletion trajectories are curved. (D) Same as (B) but for the maintenance model in (C). The regions in which the first depleted resource is resource 1 or resource 2 are shown as Ω_1 and Ω_2. (E) Model of resource consumption in which stoichiometry varies with growth rate according to changes in proteome allocation (Supplementary Information Sec. S10). This causes stoichiometry to vary with resource concentration, and so depletion trajectories are curved. (F) Same as (D) but for the dynamic allocation model in (E).

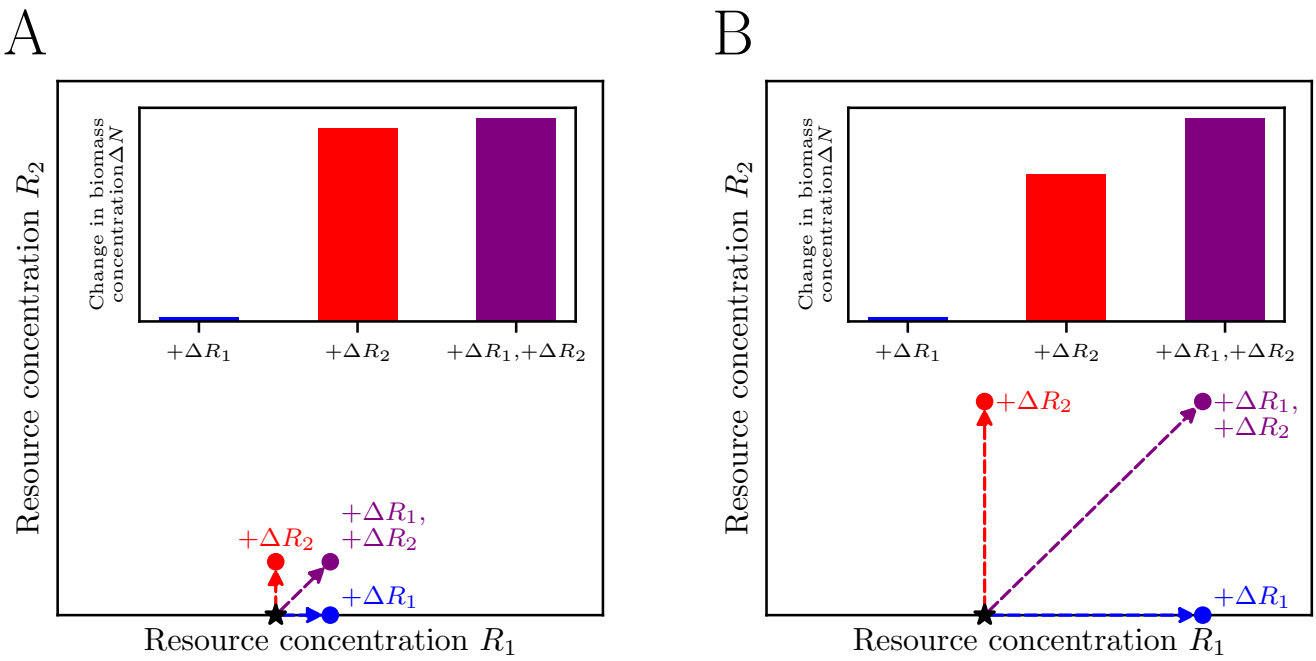

FIG. S11. **Resource supplementation outcomes with non-Liebig yield limitation.** Same as Fig. 4B,C but where biomass yield has non-Liebig dependence on resource concentrations (generalized-mean model with $q = -1$; Eq. 7, Methods, and Supplementary Information Sec. S12).

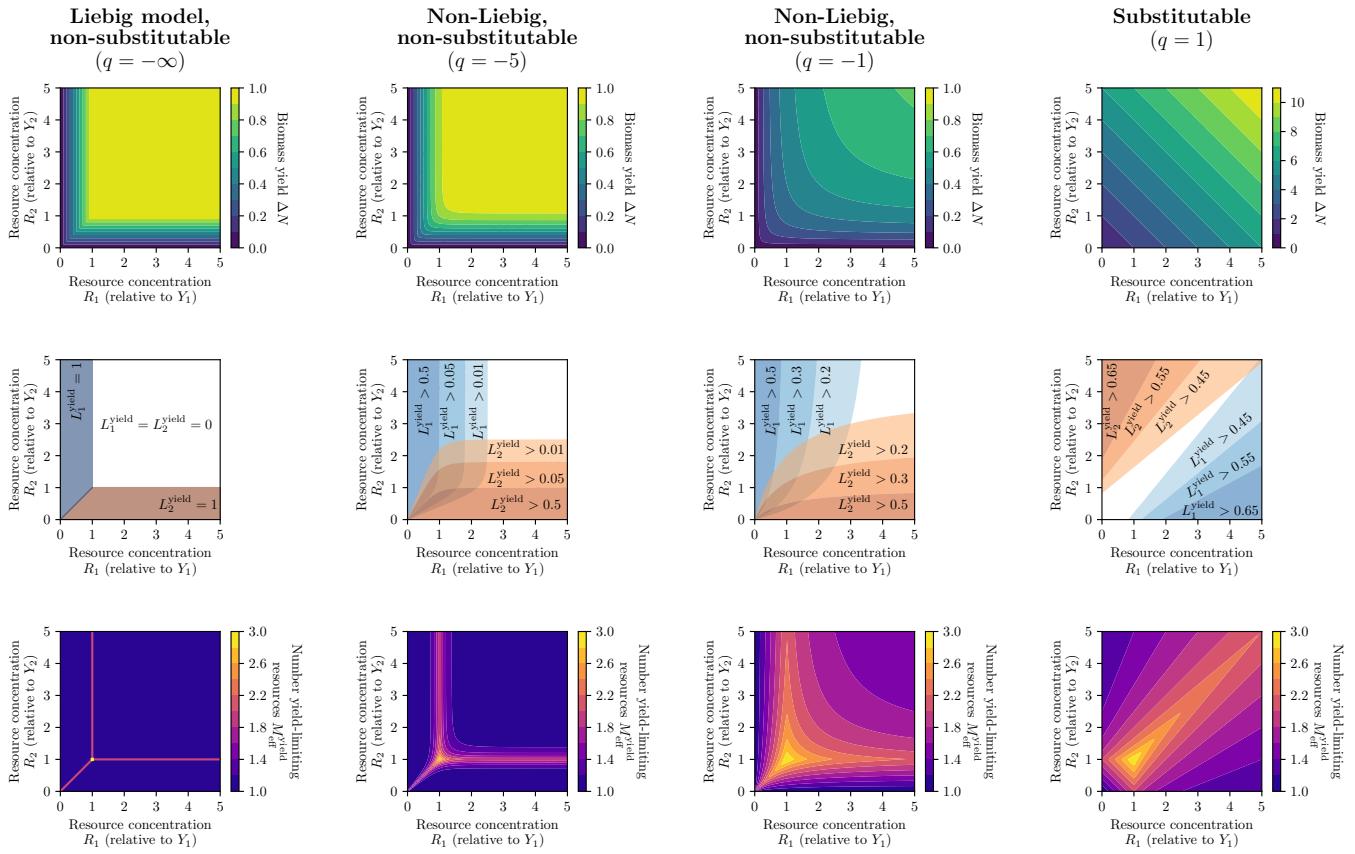

FIG. S12. **Generalized-mean model of yield limitation.** Each column corresponds to the generalized-mean model of biomass yield (Eq. 7 and Supplementary Information Sec. S12) with a different value of the resource interaction parameter q. The limit of $q = -\infty$ is equivalent to the Liebig model of biomass (Eq. 6); $q < 0$ describes non-substitutable resources, while $q > 0$ describes substitutable resources. First row: Total biomass yield over a batch growth cycle as a function of initial supplied resource concentrations R_1 and R_2. Second row: Yield limitation coefficients for resource 1 (L_1^{yield}, blue contours) and for resource 2 (L_2^{yield}, orange contours) as functions of resource concentrations. Third row: Number of yield-limiting resources $M_{\text{eff}}^{\text{yield}}$ (Eq. 5) as functions of resource concentrations. All resource concentrations R_i are scaled relative to their corresponding yields Y_i. We also assume the next most yield-limiting resource contributes biomass $R_3 Y_3 = 1$ (Supplementary Information Sec. S12).

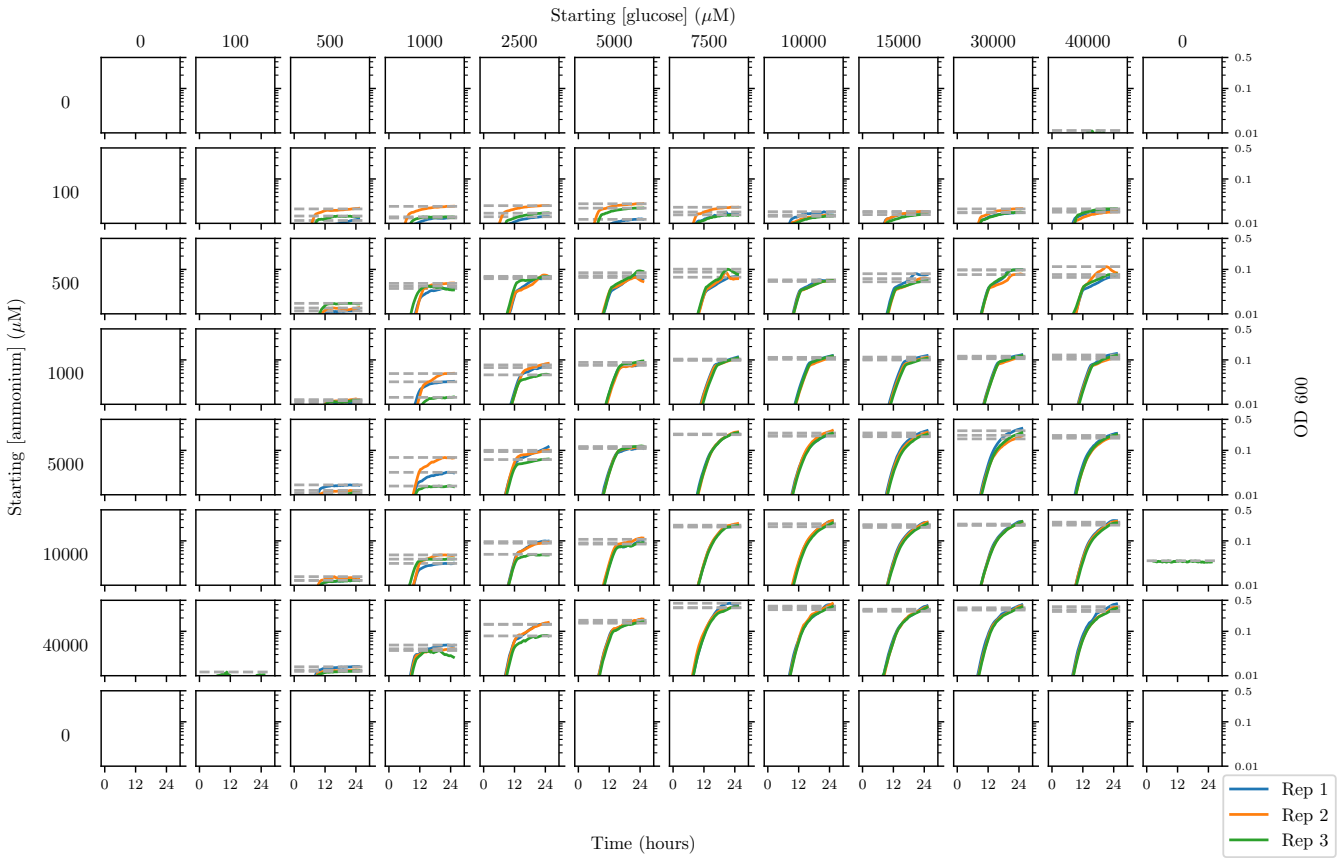

FIG. S13. **Scan of optical density growth curves across glucose and ammonium concentrations.** Growth curves of optical density at 600 nm for *E. coli* sp. MG1655 pCS-λ [55] with each well having a different starting concentration of glucose and ammonium. Triplicate growth curves are shown as colored lines; the observed biomass yields, fitted from the data, are overlayed in gray dotted lines.

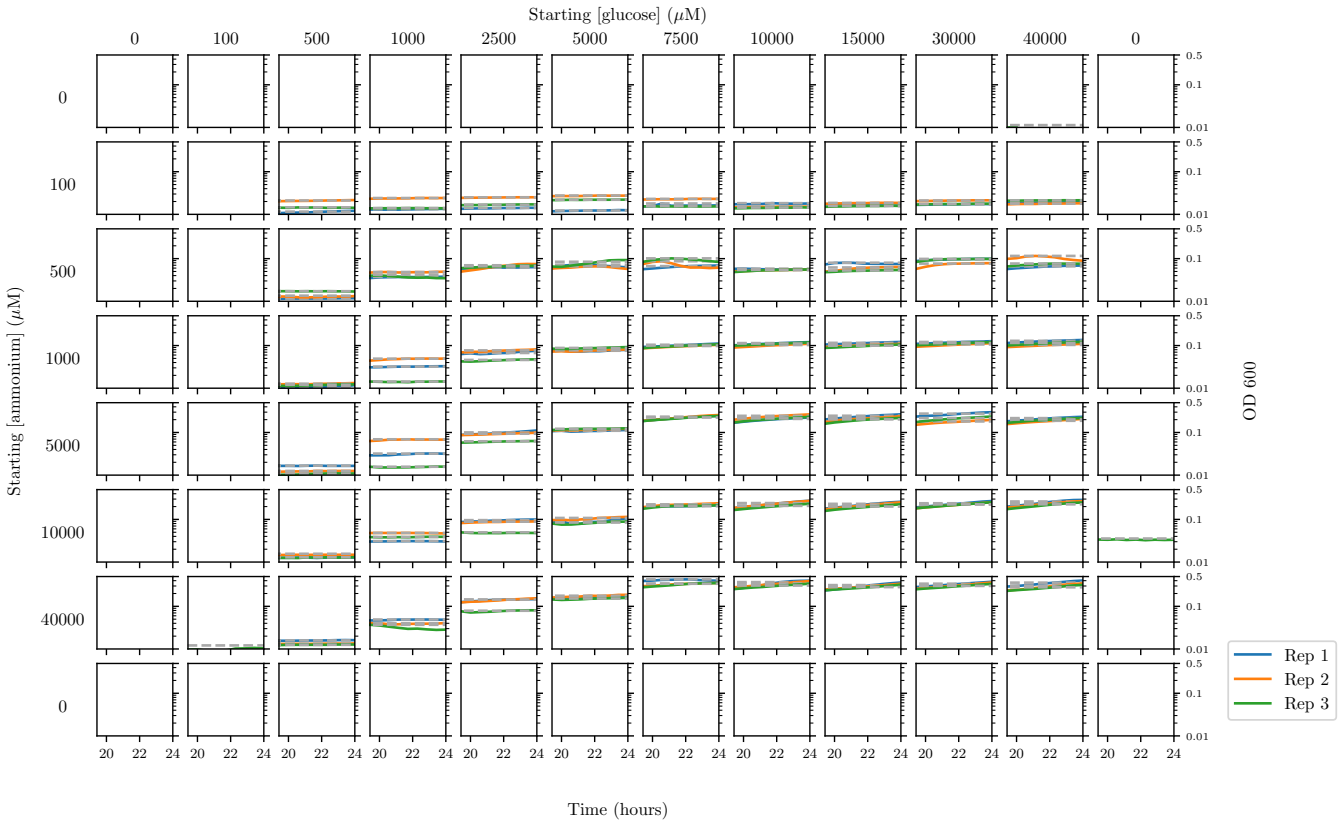

FIG. S14. **Zoomed in view of optical density growth curves across glucose and ammonium concentrations.** Same as Fig. S13 but zoomed into the time window between 20 and 24 hours where biomass yield is maximum.

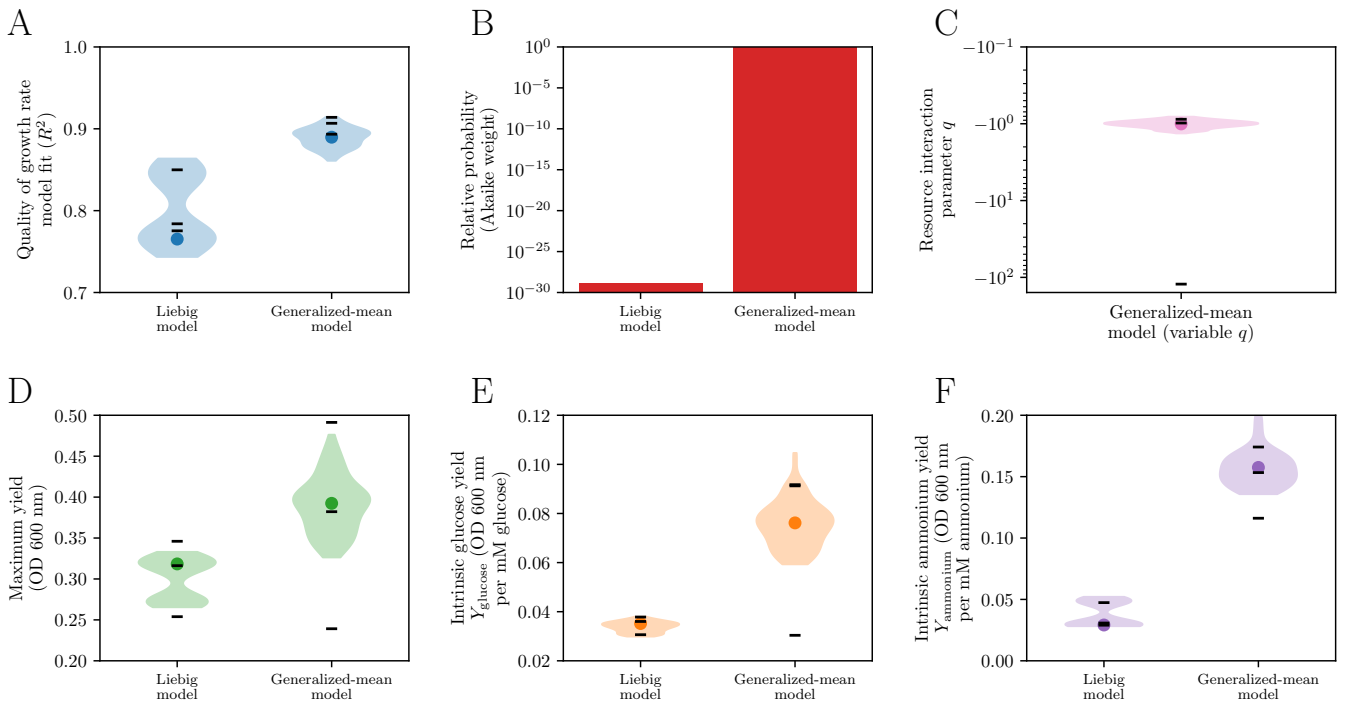

FIG. S15. **Statistics for fitting different yield models to experimental data.** We fit the Liebig model (Eq. 6) and the generalized-mean model (Eq. 7) to the biomass yield of *E. coli* as a function of glucose and ammonium concentrations (Figs. 5A, S13, and S14). (A) Quality of fit R^2 for each model. The dots represent the fit using all three experimental replicates, and the black horizontal bars represent fits for each replicate separately. The violins represent fits for 100 simulated data sets bootstrapped from the experimental replicates (Methods). (B) Relative probability of each model fit using its Akaike weight. (C) Same as (A) but showing fitted values of the resource interaction parameter q (only valid for the generalized-mean model). (D) Same as (A) but showing fitted values of the maximum yield. (E) Same as (A) but showing fitted values of the intrinsic glucose yield Y_{glucose}. (F) Same as (A) but showing fitted values of the intrinsic ammonium yield Y_{ammonium}.